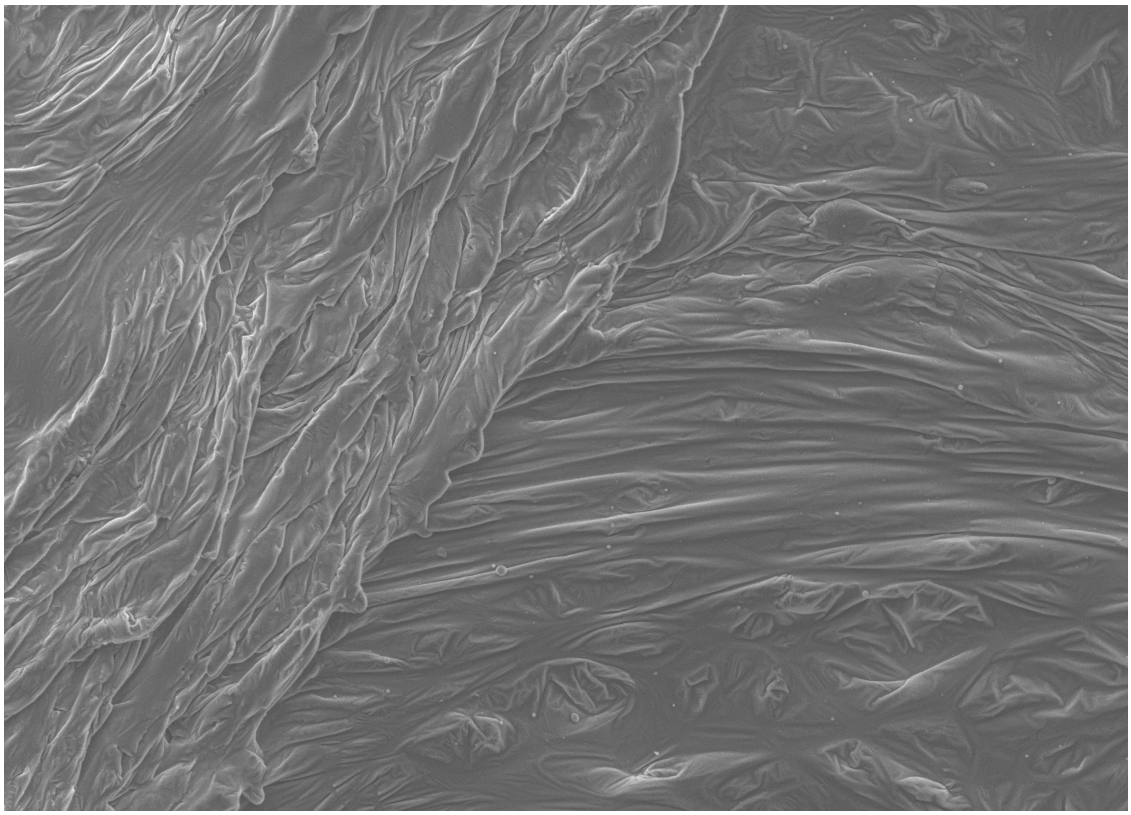

Laser Pre-Treatment of Aluminum

An investigation of the adhesive bonding after surface modification

Master's thesis in Materials Chemistry

WILMA BJÖRKMAN
HANNES SELLÉN

CHEMISTRY AND CHEMICAL ENGINEERING

CHALMERS UNIVERSITY OF TECHNOLOGY
Gothenburg, Sweden 2024
www.chalmers.se

MASTER'S THESIS 2024

Laser Pre-Treatment of Aluminum

An investigation of the adhesive bonding after surface modification

WILMA BJÖRKMAN
HANNES SELLÉN

CHALMERS
UNIVERSITY OF TECHNOLOGY

Department of Chemistry and Chemical Engineering
Division of Applied Chemistry
CHALMERS UNIVERSITY OF TECHNOLOGY
Gothenburg, Sweden 2024

Laser Pre-Treatment of Aluminum
An investigation of the adhesive bonding after surface modification
WILMA BJÖRKMAN, HANNES SELLÉN

Supervisor: Kerstin Wasmuth, Volvo Cars Corporation
Examiner: Magnus Skoglundh, Applied Chemistry

Master's Thesis 2024
Department of Chemistry and Chemical Engineering
Division of Applied Chemistry
Chalmers University of Technology
SE-412 96 Gothenburg
Telephone +46 31 772 1000

Cover: SEM-image of extruded aluminum after treatment with laser parameter T2.

Typeset in LaTeX
Gothenburg, Sweden 2024

Laser Pre-Treatment of Aluminum
An investigation of the adhesive bonding properties after surface modification
WILMA BJÖRKMAN & HANNES SELLÉN
Department of Chemistry and Chemical Engineering
Chalmers University of Technology

Abstract

This project focused on the laser pre-treatment of aluminum sheet and extruded aluminum within the 6xxx-series, applied on battery pack applications at Volvo Cars. Laser parameters were evaluated by surface characterization and lap shear testing, correlating adhesion to surface properties. Four different adhesives were investigated together with three different laser parameters. The results were compared towards untreated surfaces as well as plasma treated surfaces.

Results showed that laser effectively cleaned the treated surfaces, and that it altered the surface structure. Clean and structured surfaces was shown to improve adhesion by increasing the strength, and giving a more favorable failure mode of the adhesives. After tropical ageing, three of the adhesives increased in strength due to post curing, whereas one degraded below the desired strength.

XPS measurements showed that laser treatment induced thermal oxide growth, and confirmed cleanliness results, both enabling stronger bonding. The oxide layer thickness of untreated aluminum was 3–4 nm, while laser treated surfaces showed oxide thickness of 25–55 nm. SEM-EDX was not applicable to study the oxide layers due to insufficient resolution.

Laser parameter T2 showed the greatest potential, however new sets of laser parameters need to be studied, with a particular emphasis on a high %overlap scan.

Keywords: Structural adhesives, Aluminum, Laser pre-treatment, Lap shear testing, Surface characterization.

Acknowledgements

We would like to show our gratitude to our supervisor Kerstin Wasmuth for always answering our questions when needed. Special thanks to Roy Johansson and Surface treatment center, Lisa Lenell Lundberg and the rest of the Material Center for helping us in the lab. Thank you Esa Laurila for always being available helping us with the laser treatment.

Big thanks to Eric Tam for helping us with XPS measurements as well as interpretation of the results, and to Stefan Gustafsson for helping us with SEM-EDX analysis.

Lastly, we want to thank our friends and family for supporting us through our years at Chalmers.

Wilma Björkman, Hannes Sellén, Gothenburg, May 2024

List of Acronyms

Below is the list of acronyms that have been used throughout this thesis listed in alphabetical order:

AF	Adhesive Failure
BLT	Bond Line Thickness
CF	Cohesive Failure
EDX	Energy Dispersive X-ray Spectroscopy
LSS	Lap shear strength
PUR	Polyurethane
RFU	Relative Fluorescence Unit
SCF	Surface Cohesive Failure
SEM	Scanning Electron Microscopy
SFE	Surface Free Energy
TIM	Thermal Interface Material
VCC	Volvo Cars Corporation
XPS	X-ray Photoelectron Spectroscopy

Contents

List of Figures

List of Tables

1
Introduction

The global average surface temperature has risen by about 1.2 °C since pre-industrial levels, leading to heatwaves and other extreme weather events [1]. The pivotal Paris Agreement, forged during the UN Climate Change Conference in December 2015, aims to curtail greenhouse gas emissions, striving to cap the global temperature increase at a maximum of 1.5 °C above pre-industrial levels [2]. However, greenhouse gas emissions have not yet reached their peak [1]. To prevent catastrophic global warming, it is essential that greenhouse gas emissions reach their zenith before 2025, followed by a substantial 43% reduction before 2030 [2]. In order to achieve this, companies need to take action. To tackle this, Volvo Cars Corporation (VCC) has set a goal to be fully electric by 2030, *i.e.* only produce electric cars and phasing out combustion engines and hybrids [3]. The goal-setting of being fully electric by 2030 sets pressure on the research and production of electric cars.

Within vehicle construction, aluminum is one of the most used construction material [4] as it has good mechanical properties, low weight and low cost [5]. However, aluminum alloys are difficult to weld as they have low electrical resistance. A more commonly used technique is using structural adhesives for joining dissimilar parts in the automotive industry. Adhesives are also beneficial since they have low weight and cost [6]. However, aluminum needs to be pre-treated to enhance its adhesion properties prior to assembly, painting, and other production processes [4]. The adhesive strength depends on both the mechanical and chemical properties of the substrate and the adhesive itself. Major contributors to good adhesive properties are the surface area, surface roughness, and the wettability. There are several techniques to improve these, such as etching and pitting. A more newly explored technique to improve the bonding strength is the use of laser irradiation [7]. Laser pre-treatment is an advantageous choice of pre-treatments compared to chemical treatments since it does not require any harmful solvents which are both costly and wasteful [8]. Additionally, laser treatment has been shown to be a better option than mechanical treatments as it is more time and labor efficient [9]. Further environmental, societal, and ethical aspects of the project are found in Appendix B.1.

1.1 Aim and objectives

The aim of the thesis was to correlate the adhesion properties of laser pre-treated aluminum to the surface properties, and to deepen the understanding of the effects on aluminum from different laser parameters.

The objectives of the project were to evaluate the surface properties such as the cleanliness, roughness, and chemical composition of aluminum sheet, and extruded aluminum. The thesis investigates three different laser parameters, and how the surface properties are correlated to the adhesion strengths with four different resins. The study was also conducted on both untreated and plasma treated specimens as references.

1.1.1 Demarcations

The research was only conducted on aluminum coupons on a laboratory scale and not on a finished full scale product. This is due to the early stage of the research which requires a basic understanding of how the laser parameters modifies the surface of differently processed aluminum. This is crucial knowledge to attain before applying it in production. The time frame of the thesis was also a factor limiting the amount of considered laser parameters, adhesives, and alloys.

2
Theory

2.1 Surface properties

Surface properties of the substrate play a crucial role to achieve the desired outcome and reproducible results. These properties are the main challenge for engineers when choosing a suitable pre-treatment method. A rougher surface for instance, cause a large surface area as the adhesive can penetrate into cavities, pores or voids, leading to improved adhesion strength. Furthermore, the wettability and surface free energy of a surface are important parameters when evaluating the pre-treatment method, as the adhesive must spread over the surface to enable strong adhesion [10].

2.1.1 Surface free energy

Surface free energy (SFE) is a thermodynamic quantity determined by the state of the surface atoms of the material at equilibrium and is characteristic for every material. The SFE is the work needed to create a new surface unit while separating two phases in equilibrium. SFE can not be measured directly, but there are several methods that measures SFE indirectly including Zisman, Owens-Wendt, Fowkes, van Oss-Chaudhury-Good and Neuman. The calculations of the SFE is based on Young's equation (Equation 2.1) [11].

$$\gamma_{SG} = \gamma_{SL} + \gamma_{LG} \cdot \cos\theta \tag{2.1}$$

Where, γ is the interfacial tension between the solid (S), liquid (L) and gas phase (G) respectively and θ is the contact angle between the liquid and the solid.

The Owen-Wendt method utilizes a dispersion and a polar liquid (often diido-methane and distilled water) to determine the SFE as the surface tension and the polar and dispersion components of SFE are known. The SFE can be calculated from Equation 2.2,

$$\gamma_S = \gamma_S^d + \gamma_S^p \tag{2.2}$$

where γ_S is the surface free energy, γ_S^d is the dispersion component of SFE and γ_S^p is the polar component of SFE. The respective components (γ_S^d and γ_S^p) can be calculated based on the material's polar and dispersive components of SFE, as well as the corresponding values for water and diiodo-methane. Additionally, the calculation involves considering the contact angles of diiodo-methane and water on the substrate [11].

2.1.2 Wetting

Wetting refers to a liquid's ability to spread over a solid surface, or over another liquid with which it is immiscible. Wettability, the measure of wetting, depends on the characteristics of both the surface and the liquid. Good wettability, *i.e.* good spreading of the liquid droplet, is characterized by small contact angles (θ). This arises from strong adhesive forces between the liquid molecules and the surface. Conversely, if cohesive forces dominate within the liquid drop, it results in decreased wettability [12]. The spreading of a droplet continues until equilibrium is reached. The spreading follows Young's Equation, Equation 2.1. The interfacial tension for solids are usually referred to as surface free energy (SFE), and is often measured in mN/m [12].

As the spreading of a droplet depends on the surface forces and the properties of the material, it could be an indication of the cleanliness of the surface. Oil contaminants have a negative effect on the spreading of a water droplet, and the contact angle could therefore be an indication of the amount of soil on the surface. Contact angles of 20-25° would indicate a clean surface, while contact angles above 100° indicate a highly soiled one [13].

Wetting plays a critical role in adhesive joints, since achieving good wetting of the adhesive is essential for creating strong bonds. Effective wetting ensures that the adhesive adequately covers the surfaces being joined. Water is commonly used in measuring contact angles as adhesives often have high viscosities, complicating the testing. Despite the difference in SFE between water (72 mN/m) and polymer-based adhesives (usually between 20-30 mN/m), contact angle measurements can still provide a reliable estimation of adhesives' wetting behavior [14].

2.1.3 Adhesion

Adhesion refers to the attraction between two substances, resulting in intermolecular forces between them. The materials to be bonded are termed substrates, and once bonded, they are often referred to as adherends. Adhesion differs from cohesion, which solely involves intermolecular forces within a single substrate. The interface between the adherend and the adhesive is a critical factor when determining the mechanical properties of the adhesive bond [15].

Thermodynamically, adhesion is defined as the work required to separate the interface from the equilibrium state of two phases to an infinite separation distance. The work of adhesion of a liquid-solid system is defined as Equation 2.3

$$W_a = \gamma_L + \gamma_S - \gamma_{SL} \tag{2.3}$$

where W_a is the work of adhesion, γ is the surface energy where the subscripts L, S, SL stands for liquid, solid and solid-liquid interface [16].

2.1.4 Surface roughness

Numerous parameters come into consideration when measuring surface roughness. One such parameter is Ra, which stands for roughness average. Ra represents the arithmetic average of the peaks and valleys on a metal surface, encompassing deviations from the mean line. Larger deviations indicate a rougher surface, resulting in a higher Ra value, whereas lower Ra values signify a smoother surface [17]. While Ra provides a useful estimate of surface roughness, it is important to note that different roughness profiles can yield the same Ra value. An alternative roughness parameter, Rz, offers a different perspective. Rz measures the difference between the highest peak and the lowest valley within a sampling length, representing the maximum height of the profile [17]. Both Ra and Rz are 2D parameters, meaning that they assess the average of sampling lines. Lastly, the roughness could be measured as the arithmetical mean of the absolute value of the height within a sampling area. This parameter is abbreviated Sa. In contrast to Ra and Rz, Sa is a 3D height parameter which considers the whole area rather than a line [18]. In this thesis, Sa will be the evaluated parameter as it gives a better estimation of the substrates investigated.

Surface roughness is a crucial consideration when working with adhesives, as bonding strength is heavily influenced by the roughness of the surfaces being joined. A greater surface roughness will increase the contact area between the substrates as well as increase the mechanical interlocking [19]. However, it is important to note that increasing surface roughness does not always guarantee stronger bonding. Instead, there exists an optimal surface roughness for achieving maximum tensile strength in adhesive joints [20]. A rougher surface could reduce the extent of wetting and hence decrease the tensile strengths as the adsorption of the adhesive is reduced [21]. Improved and altered surface roughness could be performed by for instance laser treatments [22], chemical treatments [23] or mechanical treatments [24].

2.2 Adhesives

Adhesives are chemical agents maintaining interfaces between components by either or both intermolecular forces and chain entanglements across the interfaces [25]. Commonly used adhesives are thermosets based on either epoxides or polyurethanes, providing strength to structures as they minimize the movement [26].

The use of structural adhesives within the automotive industry has increased with the production of electric vehicles, as they can promote rigidity and strength in the battery pack assembly. However, joining of dissimilar parts with adhesives complicates the disassembly and recycling of battery packs, as the bonds are non-reversible. Another drawback with thermoset adhesives is that they are not recyclable and can only be recovered as energy from heat [26].

The main types of adhesives are single and two-component adhesives. An important difference between these two types of adhesives is the curing process. Single component adhesives cure upon exposure to heat, moisture, or UV-light.

Two-component adhesives can cure first when both components are mixed. The selection of adhesive should be made considering the specific conditions due to the different curing processes [27].

In temperature-varying applications, the coefficient of thermal expansion is important to consider when selecting adhesives. Different grades of expansion upon temperature fluctuations calls for flexible adhesives to avoid cracking [28]. The performance of the joint also depends on the bond line thickness (BLT), which is usually between 0.1–1.0 mm, depending on the applications and the adhesive's properties. A more brittle adhesive usually prevents failure better in a thinner bond line, whereas a ductile adhesive performs better in a thicker bond line [29].

2.2.1 Epoxy

Epoxy resins are characterized by the presence of oxirane groups. A chemical structure of an oxirane group is illustrated in Figure 2.1.

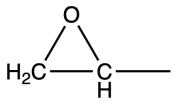

Figure 2.1: The chemical structure of oxirane

The most widely used epoxy resins are products from the reaction between epichlorhydrin and bisphenol A, which further reacts with an additional epichlorhydrin. The epoxy resin is then capable to react with various products or itself to cure and form a solid. These reaction mechanisms often occur without producing any low-molecular weight by-products. This leads to negligible shrinkage during the curing, which reduces stress in the cured structure, giving strength to the cross-linked matrix. An external cross-linking reaction occurs either by a reaction of the oxirane group with active hydrogen, typically with an amine as a hardener. Cross-linking can also occur by homopolymerization through the oxirane oxygen with the addition of a catalyst as a curing agent [30].

Epoxy based adhesives give strong bonds with high durability under various temperatures and environments. Additionally, the formula can easily be modified to control specific parameters such as toughness, flow, characteristics, cure time and temperature etc [31]. Epoxies are known to have high strength, chemical and abrasion resistance [32], excellent adhesion to metals [33], little to no volatiles during curing and low shrinkage. However they come with disadvantages such as relatively high costs, brittleness unless modified mixture, moisture absorption affecting the properties negatively and relatively long curing times [31]. Furthermore, moisture absorption can cause hydrolysis, leading to chain scission and reduction of the amount of crosslinks, further leading to irreversible degradation. Water can also lead to physical softening due to plasticization, which has shown to be a reversible degradation [34].

2.2.2 Polyurethane

Two-component adhesives based on polyurethane (PUR) are made from reacting isocyanates with polyols [35], shown in Equation 2.4. Further, isocyanates can react with hydroxyl groups on the surface on which it is applied, resulting in adhesion due to covalent bonds between the adhesive and the adherend [36].

$$\text{-NCO + -OH = -NHCOO-} \tag{2.4}$$

Hardening of the adhesive starts upon mixing, which is relatively easily achieved due to the low viscosity of the compounds. Properties such as flexibility and hardness are determined by the mass ratio of the two components. Using linear polyols in combination with a small amount of isocyanate gives a flexible bond line, while the use of a branched polyol together with a larger quantity of isocyanate gives a brittle bond line [35]. PURs can have a wide range of hardness, excellent wear, tear, chemical resistance, and high strength. It is used in applications ranging from truck wheels to shoe soles. A drawback with PURs is that free isocyanate can cause dermal and pulmonary sensitization [32].

2.2.3 Post curing

During the initial curing process, the adhesive undergoes chemical reactions to establish robust chemical bonds, known as crosslinks, between the surfaces being bonded together. However, if curing is conducted at ambient temperature, it may not reach completion, resulting in the adhesive not achieving its maximum strength. This incomplete curing can be attributed to various factors including time, temperature, and environmental conditions [37].

When a structural adhesive that has not yet fully cured is exposed to an elevated temperature, a phenomenon called post curing can occur. Post curing serves as a secondary curing process which promotes additional crosslinking within the adhesive and thereby enhancing mechanical properties such as increased bond strength, higher heat resistance and greater chemical resistance [37].

2.2.4 Water's impact on adhesive joints

Adhesive joints using structural adhesives can be sensitive to humidity, particularly when it exceeds 65%. This sensitivity is because water can diffuse into the joints, affecting their integrity [21] by disprupting the hydrogen bonds and making the adhesive more soft and flexible. This mechanism is known as plasticization [38]. The diffusion of water can be understood using the Fickian model, which relies on two key factors: the diffusion coefficient and the solubility coefficient [21].

Water is a highly polar solvent that can penetrate adhesive joints both as a liquid and as vapor. This penetration can alter the properties of the adhesive, leading to issues like swelling, crazing, cracking, or hydrolysis. However, the most significant problem arises at the adhesive´s interface. This stems form the thermodynamic work of

adhesion. Adhesive-metal interfaces in water has negative work of adhesive, which means that the interface is unstable. The instability arises from the high surface free energy of metal oxides, particularly the polar component, making them prone to disruption when exposed to water. Fortunately, suitable pre-treatment methods can enhance the performance of structural adhesive joints with metals, mitigating these issues [21].

2.2.5 Thermal Interface Material

Thermal Interface Material (TIM) is a material, often a polymer, commonly used in electric devices that generates heat. The material is placed as a bridge between the heat source and a heat removal system in order to achieve efficient heat transfer, thus avoiding operating issues. Polymeric materials are widely used as TIMs since they possess good thermal stability, adhesion, as well as electrical insulation. However, in some application fields, fillers are required in the matrix due to the low values of thermal conductivity of polymers (<0.3 W/mK). By modifying the formulation of polymer matrix and filler materials, differently desired properties of adhesion and thermal conductivity can be obtained [39].

2.3 Aluminum

Aluminum is a commonly used material in the automotive industry due to its high strength in combination of low weight. Studies have shown that the use of aluminum instead of conventional materials, such as steel, can decrease the weight by 25-40%. When reducing the weight, the fuel efficiency of a combustion engine increases, and the range of a battery increases. A drawback however, is the high price of aluminum compared to steel [40].

Aluminum is the third most abundant metal and is found in the Earth's crust. The beneficial properties and abundancy makes aluminum the second most used metal after steel. Aluminum in its pure form is relatively weak and it is therefore often alloyed to improve the strength. Alloying elements include copper, magnesium, manganese, silicon, tin and zinc. The alloying elements and the composition can be tailored depending on the desired properties and application. In addition to the low density, aluminum and its alloys offer excellent corrosion resistance, good electrical and thermal conductivities, good workability, ductility and strength. Due to its workability, aluminum can easily be shaped to any form or size.

Aluminum alloys comes in two classifications, the Non-Heat-Treatable and the Heat-Treatable. Within the Heat-Treatable, so called precipitation-strengthened, the 2xxx (copper), 6xxx (silicon and magnesium) and 7xxx (zinc) series are found. The process of the 6xxx series is as follows: casting and homogenization, hot working, cold working, annealing and ageing treatment. Hot work treatment could be for *e.g.* rolling and extrusion [41].

The 6xxx series alloys are generally considered to have good corrosion resistance compared to alloys containing copper or zinc. Moreover, they have a medium strength as they can undergo age-hardening through precipitation of magnesium silicide, making them stronger than the 5xxx series but not as strong as the 2xxx and 7xxx alloys [42]. In this project, aluminum alloys within the 6xxx series were studied, where half of the study focuses on an extruded alloy and the other half focuses on an aluminum sheet.

2.3.1 Metal processing methods

Rolling and extruding are two examples of industrial processing for shaping aluminum. Rolling involves pressing the metal between counter-rotating rolls to induce plastic deformation, where the frictional forces are crucial for initiating the rolling process, which are typically reduced using lubricants [43]. In contrast, extrusion involves pushing a metal billet through a die to obtain products with constant cross-sections, commonly used for manufacturing various shapes, especially in aluminum alloys. Hot extrusion of aluminum alloys requires pre-heating billets to high temperatures and careful control of friction to avoid surface defects. Cooling and subsequent treatments are necessary to achieve the desired mechanical properties in the final product [44].

2.3.2 Aluminum oxide

The excellent corrosion resistance of aluminum is due to the formation of a passive oxide film, alumina (Al_2O_3). When aluminum comes in contact with water, either from immersion or exposure to the atmosphere, an aluminum oxide is formed through the reaction shown i Equation 2.5 [45].

$$4Al\,(s) + 12H_2O\,(l) + 3O_2(g) \rightarrow 2Al_2O_3(s) + 12H^+(aq) + 12OH^- \tag{2.5}$$

Calculations show that Gibbs free energy for the reaction is negative, which is an indication that the oxide is formed spontaneously. The naturally formed aluminum oxide is often around 2-4 nm thick, but it can be grown thicker by anodizing techniques [45].

Aluminum oxide presents challenges for adhesive joints since the surface oxide layer can attract dirt and contaminants with low surface energy, causing wetting issues. This hinders the formation of strong bonds. A viable solution to clean the surface could involve pre-treatments such as laser ablation to enhance the adhesion properties of the surfaces [46]. Aluminum oxide has been claimed to improve adhesion by increasing the possibilities for -OH bonding [22].

2.4 Pre-treatments

2.4.1 Laser pre-treatment

Laser is an acronym that stands for "Light Amplification by Stimulated Emission of Radiation". The laser has several important characteristics such as directionality, monochromaticity, brightness and coherence [47]. Lasers are frequently utilized for surface pre-treatment, which has been efficienct in enhancing the chemical bonding strength between adhesive molecules and metal surfaces. Pulsed lasers in particular, stand out as they can deliver a substantial amount of energy within a short time frame. This rapid and concentrated energy deposition enables the modification of the chemistry, crystal structure, and morphology of the metal surface, which affects the wettability and the roughness. These two properties contribute to an improved bonding interface for subsequent adhesive applications [9].

Furthermore, laser pre-treatment offers the advantage of not using any solvents, which can be both costly and generate a substantial amount of highly polluting waste. This makes laser pre-treatment a potentially superior solution, particularly when considering its environmental impact [8]. In addition to its eco-friendly aspects, laser treatment exhibits another beneficial characteristic as it has the ability to effectively clean surfaces [9]. Laser pre-treatment can also be applied on specific areas of the surface, rather than treating the entire surface uniformly. This targeted approach not only ensures efficient material usage but also yields consistent results, thereby facilitating integration into mass production processes [48].

A drawback using lasers on highly reflective metals such as aluminum, is the reflection of the laser beam. Aluminum can reflect around 92% to 98% of the visible and infrared light, this can lead to damage of the equipment such as the fiber. To deal with the reflection, high intensities needs to be used as the absorption rate of the laser increases when the temperature increases [49].

2.4.1.1 Removal of contaminants

The laser cleaning technique which is particularly in interest for this project is dry laser cleaning. This process involves directing the laser onto the surface, inducing rapid thermal expansion of the substrate. This facilitates the removal of dirt from the surface, often referred as laser ablation. Achieving optimal cleaning without damaging the substrate requires careful consideration of laser pulse parameters. Key parameters include laser intensity and wavelength, pulse duration, repetition frequency, and incident angle. These factors collectively determine the cleaning force exerted on the surface [9]. An illustrative figure of the working principle of laser pre-treatment is shown in Figure 2.2.

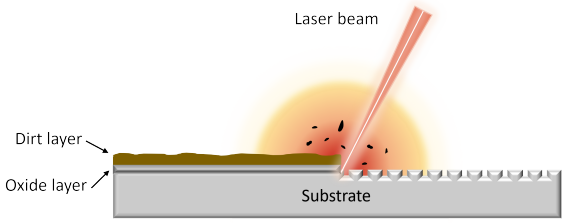

Figure 2.2: The working principle of laser pre-treatment.

Regarding the intensity and the repetition frequency, low intensities demands a high repetition frequency to achieve efficient cleaning. The main cleaning process at low intensities is due to evaporation and phase explosion of dirt, caused by laser thermal ablation. Conversely, higher intensities does not require as many pulses for equivalent cleaning. However, higher intensities may cause excessive heating leading to degradation of the substrate [9].

The interaction between lasers and materials depends on the wavelength, which is related to the electronic properties. When the energy of incoming light exceeds a certain threshold known as the band gap, single photons can be absorbed. This absorption triggers electron transitions within the material, so called excitation. Excited electrons then collide with lattice phonons, causing vibrations in the crystal lattice structure. The collisions cause disorder in the lattice, breaking bonds, leading to material removal [9].

Shorter wavelengths have higher photon energy and are more likely to cause single photon absorption, and therefore more favorable for chemical ablation. In this process, the energy from absorbed photons initiates chemical reactions leading to material removal. In contrast, longer wavelengths have lower photon energy, which are better suited for thermal ablation. In this case, the absorbed light energy primarily generates heat in the material. Longer wavelengths allow for greater penetration and promote heat diffusion within the material, leading to thermal effects such as vaporization, which result in material removal [9].

The pulse duration of the laser is important in determining light energy transformation. Nanosecond pulses or longer instantly convert light into heat, facilitating mechanisms like pressure constraint removal, spallation, and rapid thermal explosion for effective cleaning. In contrast, picosecond and femtosecond pulses operate differently, as they cannot instantaneously convert energy into heat [9].

The incident angle of the laser beam adds another layer of complexity to the cleaning process. A vertical angle may limit temperature rise due to shadowing, while an angled laser beam enhances cleaning efficiency due to increased energy absorption at the shadow interface between dirt particles and the substrate [9].

2.4.2 Plasma pre-treatment

Plasma is the fourth state of matter, referred as an ionized gas. It can be used in pre-treatments to modify the properties of a solid's surface without altering the chemistry of the bulk material [50]. Plasma can be used for cleaning solid surfaces by utilizing the high energy level to split open structures of contaminants. Further, it can be used for improving wetting and the adhesion by introducing oxygen and nitrogen-containing groups to the surface, making it more hydrophilic [51].

Plasma is obtained by electron separation from gaseous molecules or atoms, which occurs when sufficient energy from an external source is applied, or from collisions with one another [52]. To avoid drawbacks from using vacuum, such as size limitations, investment costs and the rough environment, atmospheric pressure plasmas are desired. Atmospheric plasma sources are classified from their excitation mode, these are: direct current and low frequency discharge, plasma ignited by radio frequency waves, and plasma ignited by microwaves. In this thesis, the first of the mentioned sources is used in a continuous working mode, namely a low-powered arc plasma torch. The arc plasma torch is composed of a cathode where electrons are emitted, a plasma gas injection system, and a nozzle confining the plasma [53].

2.5 Surface analysis techniques

2.5.1 Cleanliness

Cleanliness verification is a crucial step in order to ensure good adhesion properties. An easy and fast technique to measure the cleanliness is Relative Fluorescence Unit [54]. More commonly used is contact angle measurements which can measure both the cleanliness and the wettability of the surface [55].

2.5.1.1 Relative Fluorescence Unit

Relative Fluorescence Unit (RFU) is a common and easy method to measure the cleanliness of surfaces. It detects organic contamination such as oil, grease and cleaning fluid on metal surfaces. The working principle of the instrument is as follows: a UV-Light Emitting Diode (UV-LED) is used to excite the surface, and the resulting fluorescence is measured. The intensity of the measured fluorescent light is proportional to the level of contamination at the surface measuring point, a high intensity reading signifies a contaminated surface point. Apart from being able to quantify contamination levels, RFU provides quick and convenient means of detecting contaminants relative to a reference surface. The simplicity and speed makes it a practical tool for assessing surface cleanliness [54].

RFU is often employed in monitoring the cleanliness of manufactured metal parts both before and after the cleaning procedure. This ensures that surfaces are free from contaminants before advancing to subsequent stages of the manufacturing process, such as assembly, sealing, adhesive application, painting, or printing [54].

2.5.1.2 Contact angle

Contact angle measurements are commonly used to characterize the wetting properties of materials and is extremely surface sensitive. Indirectly, it could indicate oil contaminants, which would mean a more hydrophobic surface [55]. The hydrophobicity of a surface is linked to its surface energies and can be investigated using an optical goniometer. This analytical tool allows for the examination of the contact angle (θ) formed between a sessile drop and the surface [12]. The more hydrophobic a surface is, the greater the contact angle will be. A hydrophobic surface has a contact angle greater than 90° while a hydrophilic surface has a contact angle below 90° as seen in Figure 2.3.

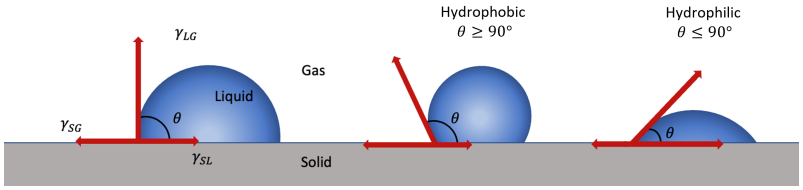

Figure 2.3: Sessile drop contact angles on a hydrophilic *vs.* a hydrophobic surface

The working principle of a goniometer is as follows: a needle disperses a desired liquid, typically water, onto the surface of the sample under investigation. A backlight is used to enhance contrast, while a front-facing camera captures images. The analysis is then conducted by the program, which calculates the mean angle from both sides of the sessile drop. Figure 2.4 shows a schematic illustration of an optical goniometer.

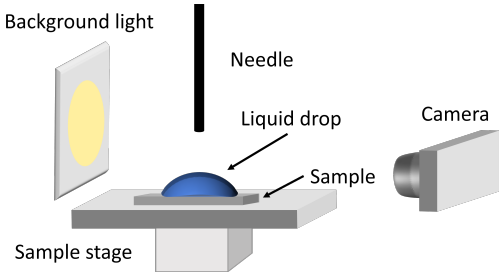

Figure 2.4: An illustration of the components within a goniometer.

2.5.2 Optical profilometry

Surface roughness is typically assessed using a profilometer. While one common technique is contact profilometry, which involves a metallic probe scanning the surface. An example of this type is atomic force microscopy. This project employs a more recently developed method, optical profilometry, where light sources scans the sample surface. The profilometer comprises two projected lights at an angle, diffracted by the surface roughness and collected on a mirror. Figure 2.5 illustrates the working principle. An image is generated by the deviation of collected light, theoretically capable of detecting roughness down to the nanometer scale. However, a limitation of this technique is its reliance on the material's ability to reflect light [56].

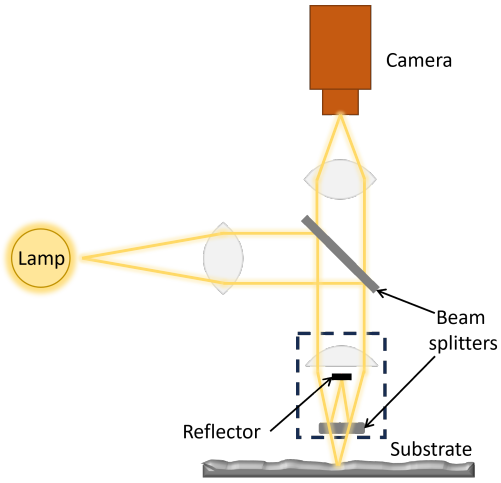

Figure 2.5: An illustration the working principle of an optical profilometer.

2.5.3 Scanning Electron Microscopy

Scanning Electron Microscopy (SEM) is a technique commonly used for characterization of the surface topography of a sample, it is also useful for investigating particle size or crystal morphology among other properties related to the surface topography. The instrument consists of an electron gun, various lenses, detectors, and a vacuum system. Depending on the instrument, it can scan surfaces with a 1 μm to 1 nm magnification. The technique is based on the interaction between an electron beam (generated by the electron gun) with the atoms of the sample [57]. The interaction can give rise to either reflection of electrons by inelastic scattering, elastic scattering, or characteristic X-rays. The reflection of electrons by elastic scattering is called secondary electrons (SE), and the reflection of inelastic scattering is called back-scattered electrons (BSE). All of these interactions, and the instrument set-up is visualized in Figure 2.6.

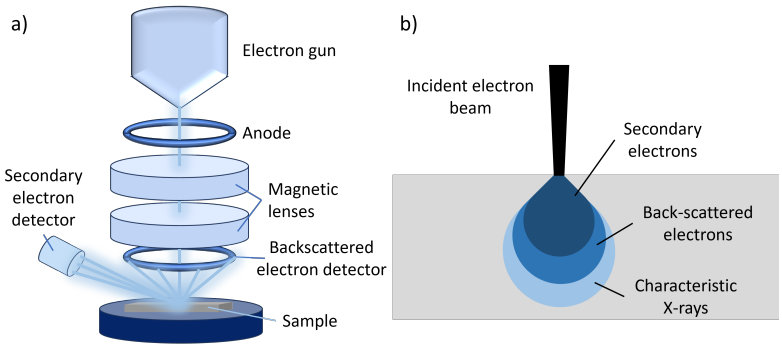

Figure 2.6: a) Illustration of a SEM set up b) the interaction of an incident electron beam with the sample.

The secondary electrons are ejected closest to the surface and the detectors, giving high contrast and information about the surface structure of the sample. Contrast differences from back-scattered electrons can reveal chemical information about the sample, since the scattering of electrons are dependent on the size of the atoms. Apart

from back-scattered and secondary electrons, characteristic X-rays are also generated, providing chemical information about the sample's identity. Moreover, the sample needs to be conductive in order to be compatible with SEM. Non-conducting materials can be sputter-coated with a conducting material, such as gold, to enable analysis with SEM [58].

2.5.3.1 Energy Dispersive X-ray Spectroscopy

Energy Dispersive X-ray Spectroscopy (EDX) is an analytical technique that is often connected to SEM. EDX can be used for identifying the composition of elements in a sample, both quantitatively and qualitatively. Quantitative analysis can be performed by analyzing the intensities of peaks in an electromagnetic spectrum, whereas the qualitative analysis is carried out by identifying the element-specific position of the peaks in the spectrum [59].

The technique requires an X-ray source that interacts with the sample, such as an electron beam from a SEM. Incident electrons from the X-ray excitation source interacts with electrons in the inner shells of atoms, causing the removal of one of these electrons. Subsequently, an electron from an outer shell transitions to fill the vacancy in the inner shell, returning the ionized atom to its ground state. This process releases the excess energy in the form of an X-ray photon, which is of characteristic energy for each element. The specific label for the X-ray depends on which electron is ionized; for instance, ionizing a K-shell electron would result in a Kα_1 X-ray. Similarly, if a vacancy occurs in the L-shell, it would be filled by an electron from the M-shell, resulting in a different label for the emitted X-ray. This cascade of transitions continues until the last shell is reached. Therefore, an atom with multiple shells will exhibit multiple emissions from a single ionization event [60]. An illustration of the EDX principle is shown in Figure 2.7.

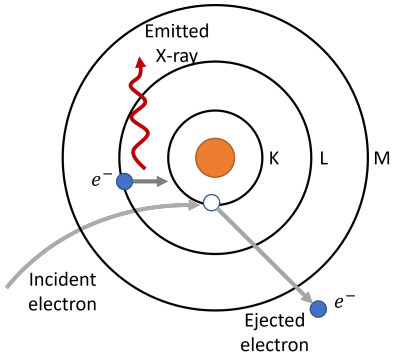

Figure 2.7: Illustration of the EDX principle.

2.5.4 X-ray Photoelectron Spectroscopy

X-ray Photoelectron Spectroscopy (XPS) is an analyzing technique used for both qualitative and quantitative chemical analysis of the top layers of a solid sample. In XPS, the surface sample is bombarded by monochromatic, soft X-ray photons,

photons of low energy (5–10 keV [61]) from an X-ray source. This is done in a high-vacuum environment (10^{-8} Torr [62]) to avoid collisions with other molecules in the spectrometer. Bombarding a sample with X-ray photons gives rise to the so called photoelectric effect, where electrons are ejected from the sample's surface atoms. The amount of ejected electrons and the kinetic energy are quantified using a photoelectron detector and an electron energy analyzer, as seen in Figure 2.8.

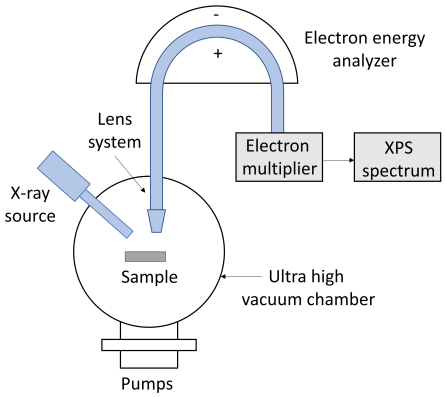

Figure 2.8: Illustration of the XPS instrument.

Further, the electron binding energy (BE_X) can be determined from the difference between the photon energy ($h\nu$) and the kinetic energy of the photoelectron (KE_P) according to Equation 2.6 [62].

$$BE_X = h\nu - KE_P \tag{2.6}$$

An XPS spectrum consists of a plot of the detected amount of photoelectrons as a function of the electron binding energy, and the chemical composition can be determined since the binding energy is characteristic for each element [63].

2.6 Lap shear test

Single lap shear testing requires two substrates that are joined together with the investigated adhesive, according to Figure 2.9. The joined substrates are put in a tensile tester, where it is loaded with a constant stress until failure [64]. The average stress at either adhesive or substrate failure can be quantified with single lap shear testing, making it possible to investigate adhesion or substrate strength [65].

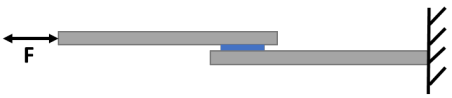

Figure 2.9: Illustration of single lap shear testing.

When conducting tests on single lap shear substrates, various failure modes may occur. One desirable failure mode is Cohesive Failure (CF), where the adhesive breaks within itself and remains attached to both sides of the substrate. A special case of CF is Surface

Cohesive Failure (SCF), where the adhesive breaks within itself, near the interface. An undesirable failure mode is Adhesion Failure (AF), which occurs when the adhesive separates from one of the adherends due to inadequate surface treatment or bonding [66]. The distinction between CF, SCF and AF is illustrated in Figure 2.10.

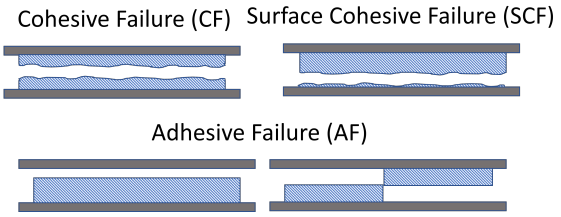

Figure 2.10: Schematic figure of CF, SCF, and AF.

To assure that the adhesive bonds can withstand severe heat and moisture conditions, a tropical cabinet can be used prior to lap shear tests, providing an environment with elevated humidity and temperature [38]. The tropical cabinet can also be used for accelerated ageing, which enables time-efficient prediction of long term exposure and the product's service life [67].

3
Methods

3.1 Pre-treatments

3.1.1 Laser pre-treatment

Laser pre-treatment of aluminum coupons was conducted utilizing two different lasers from TRUMPF, TruMicro7070 and TruMicro7060. These are Yb:YAG (λ = 1030 nm) lasers with an hourglass laser beam spot, and with a pulse duration of 30 ns. The aluminum coupons were of two different 6xxx-series alloys and processing methods, one sheet (rolled) and one extruded, both of a dimension 110x25x3 mm.

The coupons were pre-treated with three different laser parameters, with the specifics listed in Table 3.1. Laser parameter T2 and H2 were used on the aluminum sheet while parameter T2 and H6 were used on extruded aluminum. TruMicro7070 laser was used for H6 and delivered from TRUMPF, while TruMicro7060 laser was used for T2 and H2, performed at VCC Torslanda.

Table 3.1: Laser parameters used for the different laser pre-treatments.

Laser parameter	**T2**	**H2**	**H6**
Speed [m/s]	Slow	Medium	Fast
Power [W]	Medium	Medium	High
Frequency [kHz]	Low	Medium	High
Fluency [J/cm^2]	Medium	Low	High
Overlap scan [%]	High	Medium	Medium

3.1.2 Plasma pre-treatment

Plasma treatment was conducted on both sheet and extruded coupons. OpenAir® plasma from Plasmatreat was used with a program designed for adhesive fixture plates. This assured complete treatment of the entire surface of the coupons. The power of the plasma was 450–550 W, with an airflow set to 35 l/min, a movement speed of 50 mm/s, a pre-treatment width of 4 mm, and a nozzle-substrate width of 10 mm. Analysis and further procedures including the plasma treated samples was conducted immediately, or as soon as possible after plasma treatment to ensure surface cleanliness and activation.

3.2 Surface analysis

3.2.1 Relative Fluorescence Unit

RFU was measured using a SITA CleanorSpector. Six repeating measurements were conducted on different parts of the coupon and the result is based on the mean value of the six measurements. For the untreated samples, five different coupons were investigated since the result varied between the samples.

3.2.2 Contact angle

Contact angles measurements were performed using KRÜSS ADVANCE 1.6.1.0 Mobile Surface Analyzer measuring Double Sessile Drop. Distilled water and diiodo-methane were used as liquids with a dispersion volume of 1 μl. The contact angles were taken 5 s after the dispersion for the untreated and plasma treated surfaces to ensure equilibrium of the spreading. Laser treated surfaces were measured after 1 s due to fast wetting of the surface.

3.2.3 Surface roughness

The surface roughness was investigated using a non-contact 3D optical profilometer, Keyence VR-5000 Series, with a projected light in a 35° angle. The focus was automatically adjusted by the instrument and a high pass filter of 0.8 mm was used. Measurements were performed on all treated and non-treated coupons.

3.2.4 Scanning Electron Microscopy - Energy Dispersive X-ray Spectroscopy

SEM-measurements of the surfaces were conducted using the JSM-IT300 from JEOL, analyzing the secondary electrons. One coupon of each alloy and treatment type was separately mounted in the instrument with double-sided tape. Every sample was scanned at a magnification of 30x and 1000x, with an electron beam of the potential 7 kV.

SEM imaging and EDX analysis of the cross-section were performed using a FEI Quanta 200 equipped with an Oxford X-Max EDX detector. Images were acquired in the secondary electron mode using an accelerating voltage of 20 kV. EDX spectra were also acquired at 20 kV and analyzed using the AZtec software. The sample preparation prior to analysis is described in Appendix A.1.

3.2.5 X-ray Photoelectron Spectroscopy

XPS was carried out using the VersaProbe III 5000 from Physical Electronics (PHI), in which the X-ray source is a monochromatic Al X-ray, with a beam size diameter of 100 μm. The samples were scanned with a survey scan mode (with a detection limit of 1 atomic%) to evaluate the overall composition. They were also scanned with a

narrow scan to evaluate the chemical state of individual elements in a selected region. The oxide thickness was investigated by revealing the depth profile from step wise scanning the overall composition at different depths. The sputter depth was given in reference to tantalum oxide (Ta_2O_5), and the thickness was therefore multiplied with 0.62 to convert it to a scale for a Al_2O_3.

Untreated aluminum sheet and extruded aluminum coupons were cut to a size of 25x25 mm to fit in the sample chamber of the instrument. Some of these cut samples remained untreated, while others were pre-treatment using laser parameters T2 and H2. Coupons treated with parameter H6 were carefully cut into pieces after the treatment due to external delivery of H6 coupons. The samples were stored in aluminum foil and cleaned with ethanol prior to measurements with XPS.

3.3 Adhesive application method

A teflon string was put in the center of a fixture plate as a protection for adhesive residue. Coupons were put in the fixture plate with two strings of teflon on top of the coupons, leaving a gap where the adhesive was applied using a glue gun powered by compressed air. The teflon string thickness hence decides the adhesive's Bond Line Thickness (BLT). Secondary coupons were put on top of the adhesive, which were then immobilized with screw nuts, secured to 13 N. All the steps are shown in Figure 3.1. The coupons were left to cure in a fume hood for a week.

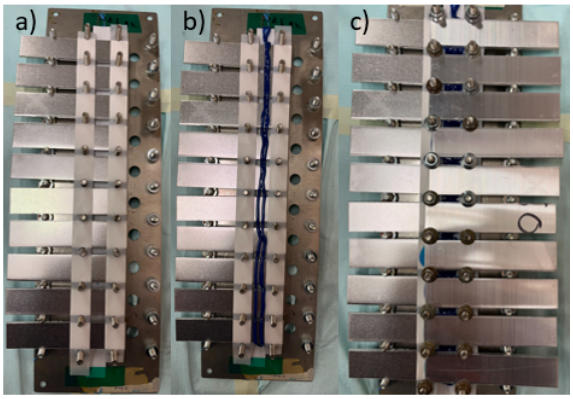

Figure 3.1: a) Coupons fixated in the fixture plate with the teflon strings b) addition of adhesive on the coupons c) attachment of the secondary coupons as well as screw nuts.

For the aluminum sheet, PUR-TIM adhesive 1 and 2 were used, with a BLT of 0.5 mm. While epoxy-based adhesive 3 and PUR-based adhesive 4 were used for extruded aluminum. Adhesive 3 and 4 were applied with a BLT of 0.2 mm and 1 mm respectively. A total of 20 coupons (10 pairs) were assembled for each parameter and adhesive type. Within each set, half were designated for immediate testing after curing, while the remaining half were allocated for studying ageing effects. This resulted in a total of 320 coupons being joined and analyzed.

3.4 Tropical ageing

Joined coupons were left to age for eight weeks in the tropical cabinet. The tropical cabinet ensures an environment with high humidity and cycled elevated temperature. After ageing, the coupons were taken out of the cabinet and sealed in zip lock bags, keeping the moisture. They were left in a constant-room for two hours, cooling down in a controlled environment prior to lap shear experiments.

3.5 Lap shear

Lap shear experiments were conducted on all joined samples. Experiments were carried out directly after the adhesive was cured in ambient temperature, and after ageing in a tropical environment. The coupons were pulled with a tensile speed of 10 ± 2 mm/min until failure using the Zwick Z050 tensile tester.

4

Results and Discussion

4.1 Lap shear test

In this section, the failure modes and lap shear strength (LSS) curves for untreated, plasma treated, and laser treated samples are presented. The results are presented for both unaged as well as samples aged for eight weeks. This is done to investigate how the adhesives' properties change when exposed to elevated heat and humidity.

The LSS curves for samples treated with laser parameter T2 and joined with the different adhesives are shown in Figure 4.1. The different curves display the deformation behavior and strength of the different adhesives without any ageing. The rest of the LSS curves are found in Appendix A.2. From the figure, it can be observed that the epoxy-based adhesive 3 (AD3) is very strong and quite brittle, while the PUR-based adhesive 4 (AD4) is weaker but tougher and more flexible. The two PUR-TIM's adhesive 1 and 2 (AD1 and AD2) are less tough than AD4 and weaker than AD3. This could originate from the conductive additives in TIM-adhesives, which can weaken interactions in the polymer matrix. Although the different adhesives show different strengths and stress response, it is important to consider that they are designed for different purposes. The suitability of an adhesive should be assessed for its intended application, rather than comparing the strengths between different adhesive types.

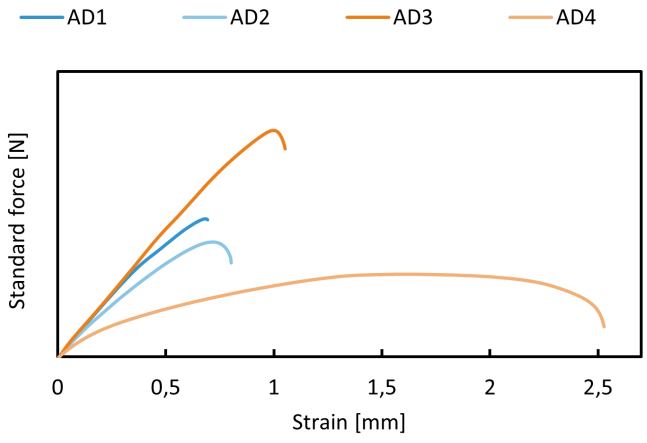

Figure 4.1: Lap shear curves for laser parameter T2 after eight weeks of ageing.

4.1.1 AD1

The lap shear results for the untreated, plasma treated, and laser treated samples using AD1 adhesive on aluminum sheet are shown in Figure 4.2. The figure shows the strength before and after eight weeks of ageing. It is evident that AD1 degraded during ageing, as its strength decreased significantly for all treatments. This is likely to be due to moisture uptake of the adhesive, leading to plasticization [38] and hydrolysis of the adhesive [21]. Furthermore, the adhesive strength is less than the VCC requirement according to VCC standards. Additionally, it did not meet the requirement of maximum 20% loss of strength after ageing.

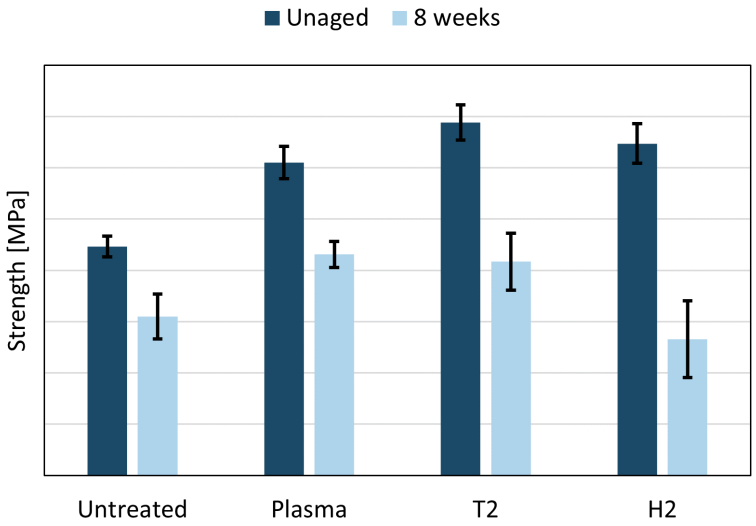

Figure 4.2: The lap shear results before and after eight weeks ageing for aluminum sheet using the AD1 adhesive.

Moreover, the failure modes of each sample with AD1 are shown in Figure 4.3. Since only the weaker failure modes SCF and AF are observed while CF is not, it is clear that none of the investigated pre-treatments in combination with AD1 is enough to fulfill the desired outcome regarding adhesive failure modes. However, notably the plasma treatment worked better than the rest of the adhesives which showed 100% SCF, but as mentioned before, it did not reach the desired strength.

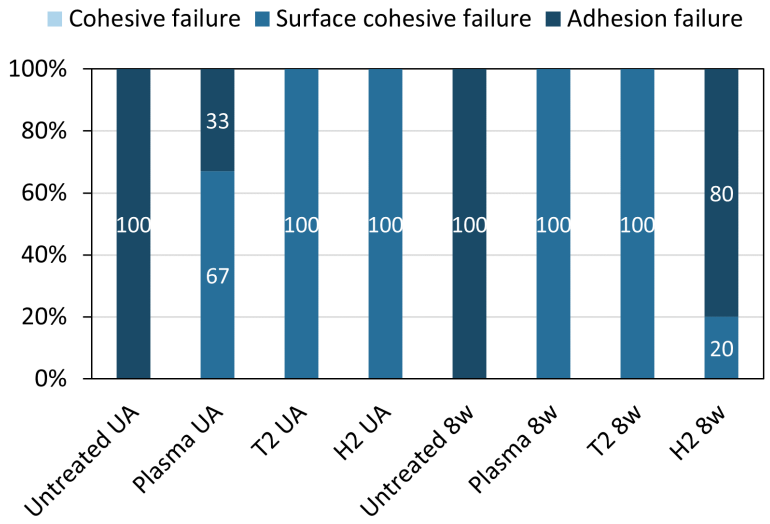

Figure 4.3: Failure modes for AD1.

4.1.2 AD2

Lap shear results for the samples using AD2 on aluminum sheet are shown in Figure 4.4. The results show that there is very little to no degradation of the adhesive after ageing. It can therefore be concluded that the adhesive withstands moisture well. As seen in Figure A.2 in Appendix A.2, the laser treated and aged samples show a prolonged curve with a longer strain. This is evidence of plasticization where the adhesive becomes more flexible, which is one of the impacts water can have on adhesives joints [38].

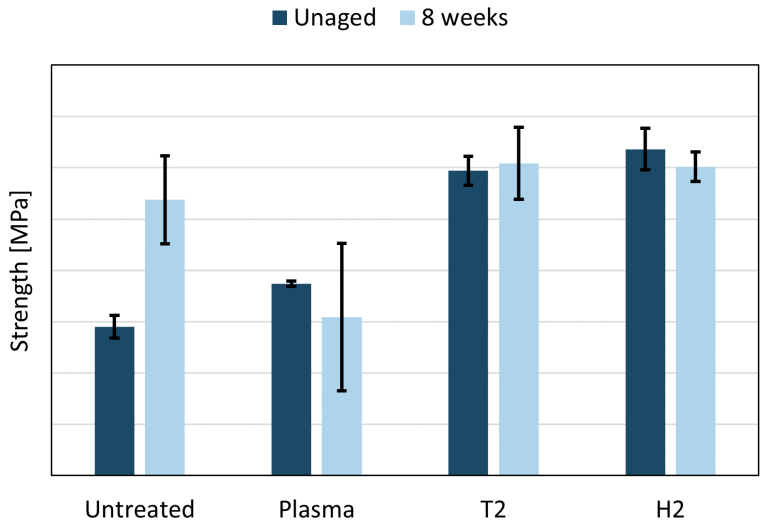

Figure 4.4: The lap shear results before and after eight weeks ageing for aluminum sheet using the AD2.

Furthermore, the failure modes are shown in Figure 4.5. It is evident that the H2 parameter would be the best choice for AD2, as it shows high strength and 100% CF after ageing. However, the T2 parameter could also be an alternative for this adhesive as it shows high strength as well as a high percentage of CF in combination with SCF.

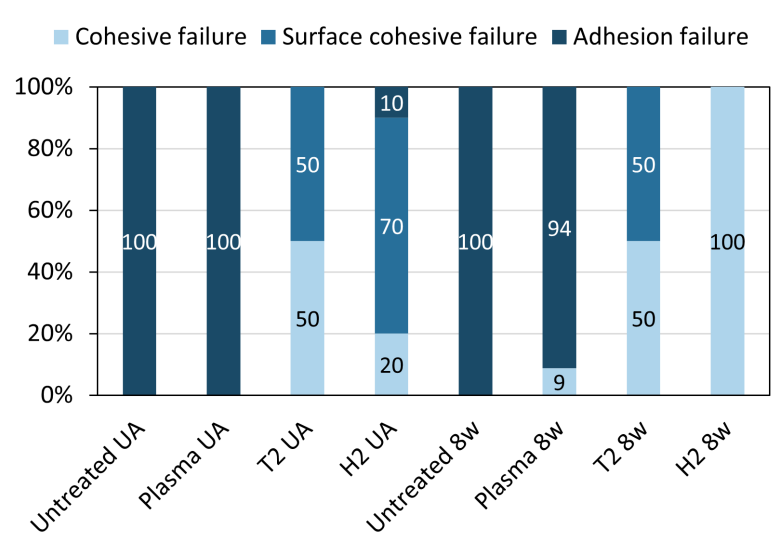

Figure 4.5: Failure modes for AD2.

4.1.3 AD3

The lap shear results for the samples using the AD3 adhesive on extruded aluminum are shown in 4.6. It is observed that pre-treatments are very advantageous as the strengths are around 4 times higher than the untreated samples' strength. It is also clear from Figure 4.6 that the strength after ageing has increased, and a postcuring process has occurred due to the elevated temperature in the tropical cabinet. Furthermore, the LSS curve (Figure A.3 in Appendix A.2) for T2 shows some plasticization as the strain increases with almost 40%.

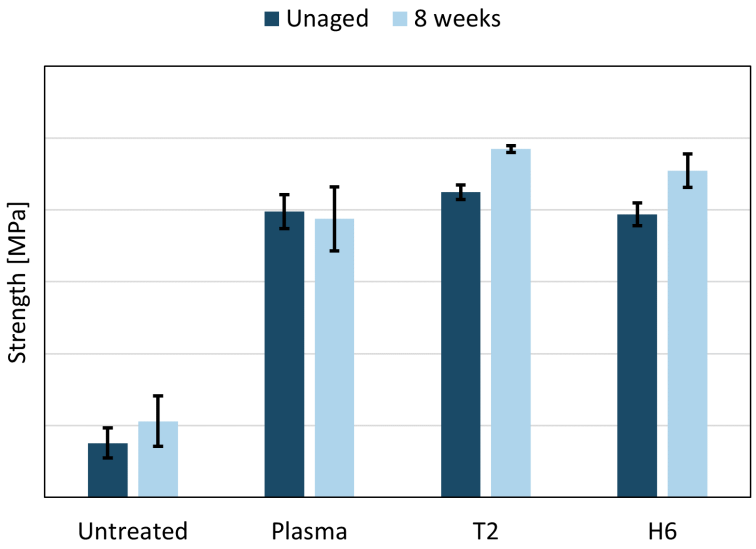

Figure 4.6: The lap shear results before and after eight weeks ageing for extruded aluminum using the AD3 adhesive.

Moreover, the failure modes are presented in Figure 4.7. Conclusion from the results would be that T2 is the best laser parameter for this adhesive, as it has the highest degree of CF as well as the strongest response to stress. However, H6 also shows high strength and acceptable results with 90% CF after ageing.

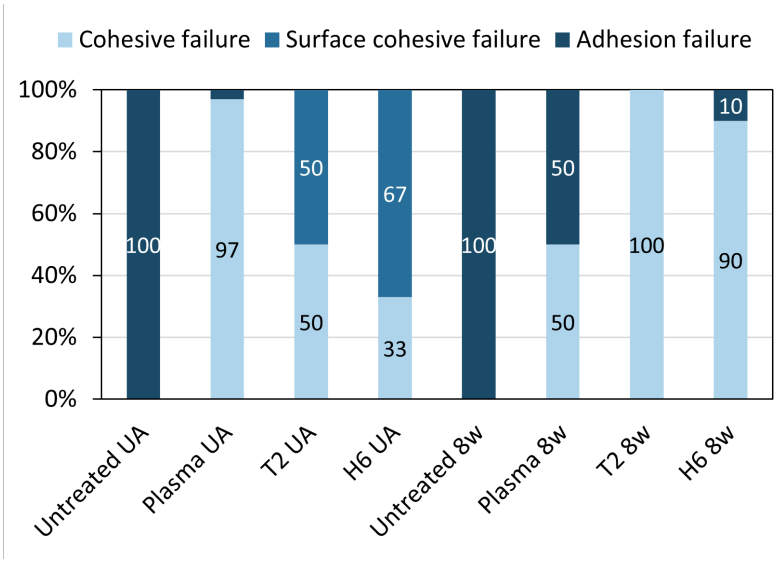

Figure 4.7: Failure modes for AD3.

4.1.4 AD4

The lap shear results for the samples using the AD4 adhesive on extruded aluminum are shown in Figure 4.8. The results indicate a high degree of postcuring as the strength is 50-60% higher for the aged samples. The LSS curves in Figure A.4 indicate that the adhesive is very flexible which may be due to the fact that it is a PUR based adhesive

in combination with a thick BLT. LSS curves also show that the strength increases with ageing, while it loses about 20% of its flexibility.

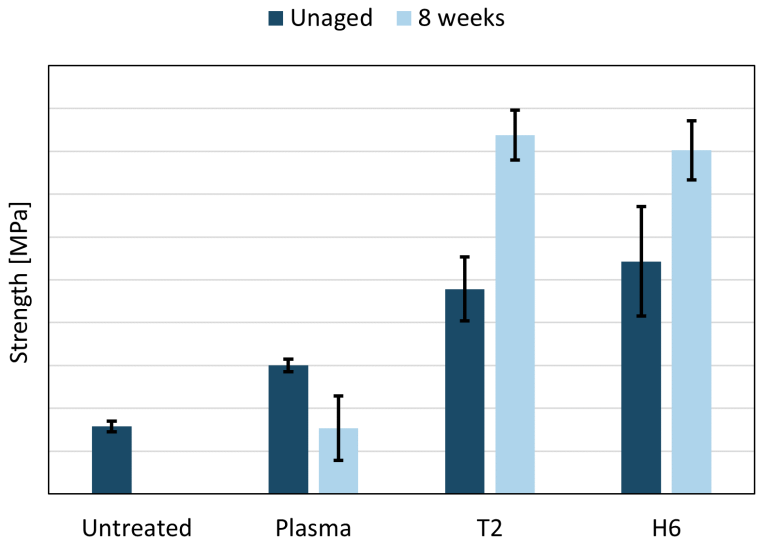

Figure 4.8: The lap shear results before and after eight weeks ageing for extruded aluminum using the AD4 adhesive

The failure modes are illustrated in Figure 4.9. It is clear that the adhesion to the substrate is not very good as no CF is shown after ageing. This is probably due to water affecting the interface between the adhesive and the substrate.

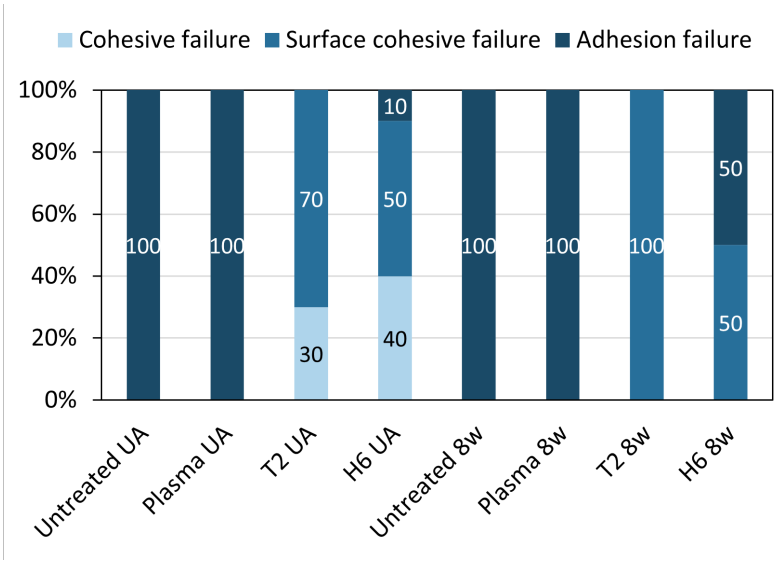

Figure 4.9: Failure modes for AD4.

During testing for AD4, the tensile tester did not pull until complete failure, requiring manual separation of the coupons for failure mode inspection. Given that the AD4 adhesive is a type of PUR adhesive known for its flexibility, manual pulling could induce some adhesive "peeling", potentially leading to less desirable failure modes.

For the future, adjusting the settings of the tensile tester to continue pulling until complete failure of the adhesive would be necessary for more accurate testing and analysis.

4.1.5 Evaluation of pre-treatments

The failure modes for the aged samples are shown in Figure 4.10. It is evident by the results that laser pre-treatment is essential to achieve cohesive breaks. Furthermore, plasma did not show any major improvement in failure mode, except for AD3, where it could be an alternative and cheaper pre-treatment method. However, using a universal pre-treatment method is preferred to keep investment costs down. Therefore, laser treatment would be the optimal choice since it effectively enhances the substrates' bonding to all four adhesives.

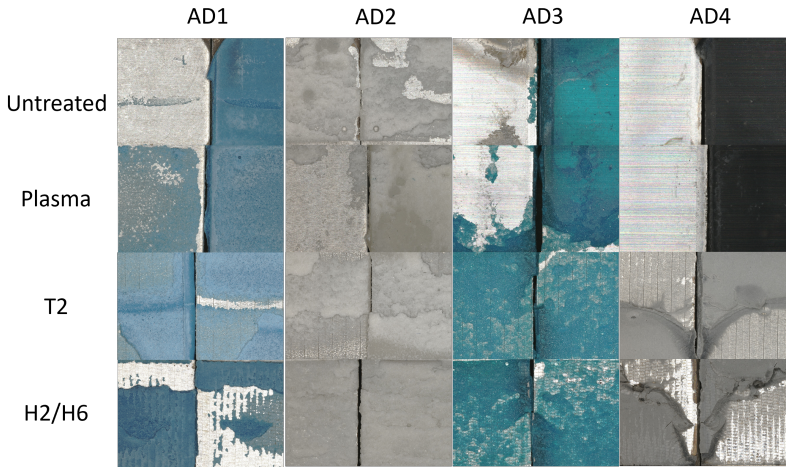

Figure 4.10: Failure patterns after lap shear testing of samples being aged for eight weeks.

From the LSS results and failure modes, the main observation would be that T2 is the best alternative of the investigated parameters as it showed no AF. Although the T2 parameter worked for all adhesives, this parameter is much slower compared to H2 and H6. It would be desired to study a new combination of laser parameters that only generates CF at a high speed. Furthermore, the ageing tests performed after eight weeks appear to simulate too harsh conditions for battery applications. A small study of a few coupons aged for only four weeks were conducted, and the results are presented in Appendix A.2.2.

4.2 Relative Fluorescence Unit

The cleanliness was investigated with RFU measurements and the results are shown in Figure 4.11. The results show that the laser pre-treatment method effectively cleans the surface from oil contaminants, since the values for the untreated and plasma treated surfaces are much higher. For the untreated material, there was a large difference between each sample, which could be due to material handling. Moreover,

since the coupons are two years old, they may have been exposed to various environments, further influencing their cleanliness. There is also a clear difference between aluminum sheet and the extruded aluminum, which can be explained by the different processing methods, as the extrusion process does not use any lubricants compared to the rolling process. The highly soiled surfaces for the untreated samples, could be one explanation for the poor adhesion observed in the failure modes across all adhesives. The soil can potentially form a barrier layer on the surface, preventing effective bonding by creating a physical obstacle.

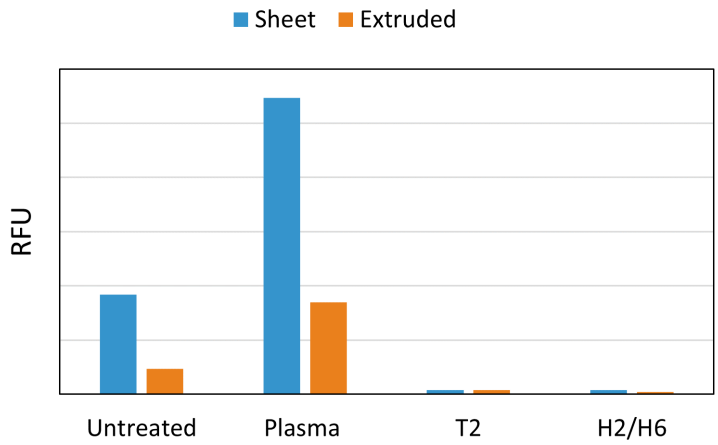

Figure 4.11: RFU values for aluminum sheet and extruded aluminum for respective pre-treatment method.

The RFU values obtained from plasma treated samples demonstrate a notable increase. Plasma-based cleaning relies on contaminant vaporization, and larger contaminants may not fully evaporate due to insufficient energy from the plasma. Consequently, they remain activated and might disintegrate into several smaller fractions, contributing to the elevated RFU values observed. The inadequacy of plasma energy might be due to both power and speed. Research indicates that high power and/or slow speed enhances cleaning efficiency. For instance, Bónová et al.'s study found that a power of 700–800 W and a speed of 5.5 mm/s effectively removed all oil from substrates. In this study, half the power and ten times the speed are employed, which could explain the inefficiency of plasma cleaning [68].

The lap shear results further confirm the inefficiency of the plasma cleaning process, as the strength of the adhesive bond is lower than the strength observed on laser treated surfaces. Nevertheless, there appears to be a small enhancement in adhesion of plasma treated coupons compared to the untreated samples, which could be attributed to some degree of surface activation. While this effect was seen for AD1 and AD3, it was not as significant for AD2 and AD4. This variation could be due to differences in the amount of soil on the samples.

4.3 Contact angle measurements

The contact angles for untreated and treated samples were measured with both distilled water and diiodo-methane. The results are displayed in Figure 4.12. Worth noting, are the results for the sample pre-treated with laser, which are taken after 1 s compared to the reference results, which are taken after 5 s. These results show large deviations due to hysteresis and non spherical shapes of the droplets from fast wetting, hence they are not trustworthy. Overall, the results clearly show that the contact angles for the untreated surfaces are much larger than those for laser-treated surfaces, which aligns with the RFU measurements showing that the untreated surfaces are covered with soil. The reduction of contact angles confirms effective laser cleaning, which is consistent with previous studies [10]. For plasma samples, high contact angles are measured, which is an indication of an inefficient cleaning. This could be due to the same reasoning as with the RFU results. Another explanation could be surface recontamination, which is instantaneous after a surface is cleaned with oxygen plasma and exposed to ambient atmosphere [69].

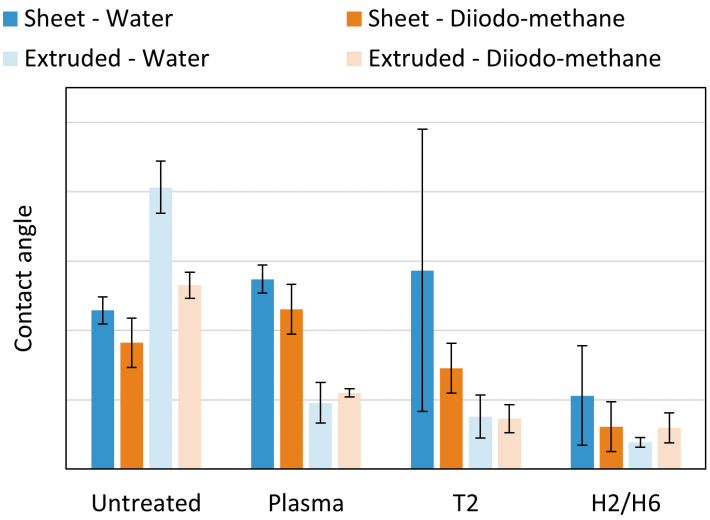

Figure 4.12: Contact angles for aluminum sheet and extruded aluminum using water and diiodo-methane as dispersing liquids.

The surface energy was measured and automatically calculated from the contact angles of diiodo-methane and water, and the results are shown in Figure 4.13. The results clearly show that the SFE increases after laser pre-treatment. However, large deviations in the contact angle also give large deviations of the SFE. The SFE of the pre-treated surfaces are between ~60–80 mN/m which indicates that polymer-based adhesives, which usually have a SFE of 20–30 mN/m [14], will wet the surface readily. As described earlier, untreated coupons' cleanliness can vary a lot from one another, and give uncertainty in the contact angle and SFE results. To improve the experiment, contact angle measurements would have to be done on several different untreated samples.

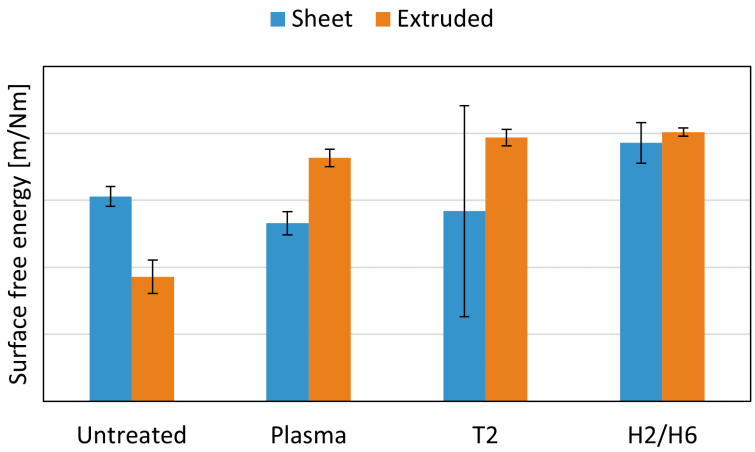

Figure 4.13: Surface free energy for extruded and aluminum sheet using water and diiodo-methane as dispersing liquids.

As indicated by the SFE results, there appears to be no hindrance for the adhesives to wet the surfaces adequately. Additionally, during the preparation of coupons for adhesive joining, the pressing action forces the adhesive to spread out, further facilitating wetting. Therefore, wetting does not pose an issue for any of the samples. However, the findings from the contact angle measurements aligns with the results from the surface free energy tests. As previously mentioned, the presence of a soil barrier could be the primary obstacle when attempting to join the pieces together, resulting in poor adhesion of the untreated surfaces.

4.4 Surface Roughness

The surface roughness was studied with an optical profilometer, obtaining values of Sa, displayed in Figure 4.14. It can be observed that untreated and plasma treated aluminum have low values, which was expected from the structure, shown in Figure 4.15 and 4.16. Theoretically, values for plasma-treated coupons should be the same as the references as plasma cleaning should not alter the surface structure. This is however not the case, most probably due to sample deviation as mentioned. As plasma treatment did not show any significant change in roughness, plasma treated specimens were not investigated using SEM or XPS.

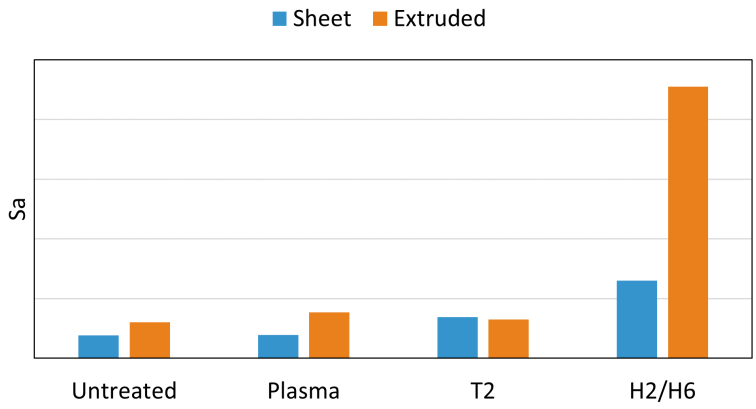

Figure 4.14: Sa for aluminum sheet and extruded aluminum of respective pre-treatment.

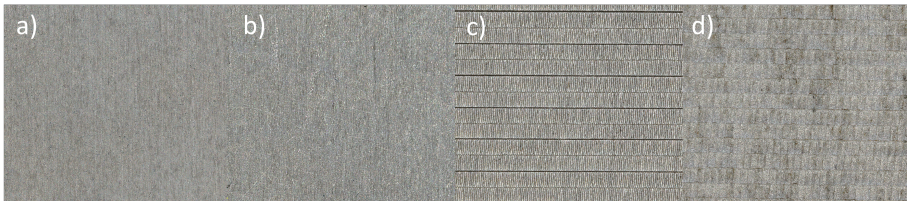

Figure 4.15: Images taken with Keyence VR-5000 Series showing the surface structure of a) untreated b) plasma c) T2 d) H2 aluminum sheet substrates.

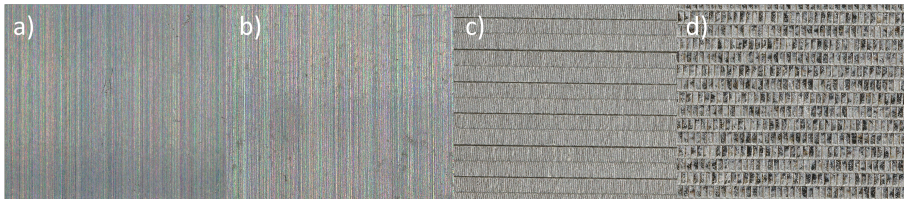

Figure 4.16: Images taken with Keyence VR-5000 Series showing the surface structure of a) untreated b) plasma c) T2 d) H2 extruded aluminum substrates.

The substrates pre-treated with laser parameter T2 has slightly lower values of surface roughness compared to H2 and H6, and even to the plasma for extruded aluminum. This can be explained by the fact that the laser can make the surface more uniform than its initial state by evening out scratches and irregularities. It can be observed that extruded aluminum treated with H6 has a higher value of surface roughness than the other parameters, caused by the high power of laser parameter H6. Previous studies have shown that high laser power leads to a high energy density at a given area, resulting in larger and deeper ablation structure. A fast laser scanning speed has the opposite effect as the material will be irradiated for a shorter time period, leading to lower surface roughening. The conclusion from the study was that the laser power is the most dominating parameter of ablation [10], which agrees with the results for the extruded aluminum, as the laser power for H6 is doubled compared to T2.

Previous studies have also shown that a greater %overlap scan results in higher surface roughness [70]. However, for the aluminum sheet material, H2 was the roughest sample, contradicting the explanation regarding both the speed and %overlap scan. Therefore, studying the Sa parameter might not be sufficient. There are several other surface roughness parameters that takes the surface structure into consideration and it might hence be advisable to consider other surface roughness parameters, for example Surface skewness (Ssk) which takes the asymmetry into consideration [71].

The lap shear results indicate that the T2 laser parameter achieved the highest overall adhesion, despite not being the roughest surface treatment. This observation aligns with findings from previous studies, as mentioned in Section 2.1.4. The study demonstrated that there exists an optimal roughness for adhesive bonding and a rougher surface does not necessarily facilitate a stronger bonding [20]. Therefore, an additional study would be necessary to determine the optimal roughness and understand the underlying trend. The study would involve investigating different degrees of roughness and analyzing the adhesion behavior towards the various adhesives.

4.5 Scanning Electron Microscopy

The top view images of untreated, T2, and H2 aluminum sheet coupons are shown in Figure 4.17, while untreated, T2, and H6 extruded aluminum coupons are presented in Figure 4.18, captured at magnifications of 30x and 1000x. These images reveal minimal structure variation on the untreated surfaces, consistent with the surface roughness measurements.

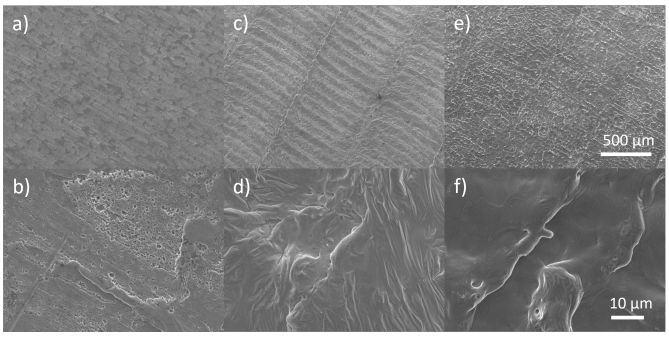

Figure 4.17: Top view SEM image of aluminum sheet: a) untreated 30x b) untreated 1000x c) T2 30x d) T2 1000x e) H2 30x f) H2 1000x.

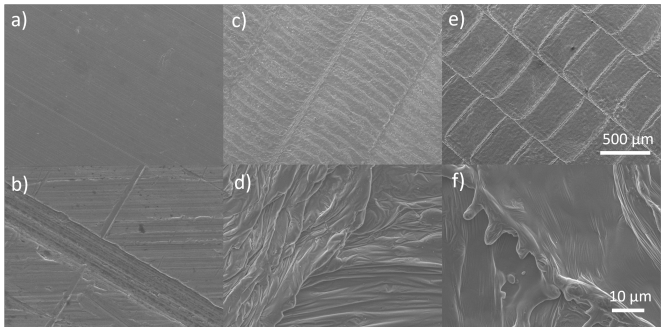

Figure 4.18: Top view SEM image of extruded aluminum: a) untreated 30x b) untreated 1000x c) T2 30x d) T2 1000x e) H6 30x f) H6 1000x.

The T2 laser parameter on both alloys reveals a consistent and evenly distributed structure across the surface, aligning well with the surface roughness results. In contrast, the H2 and H6 laser parameters result in larger melted aluminum structures, significantly impacting surface roughness compared to the T2 parameter. This difference in surface structure suggests that the T2 parameter could facilitate the formation of numerous smaller mechanical interlocks with the adhesive, potentially enhancing the strength and the CF, which can be observed in the lap shear test results.

4.5.1 Cross-section SEM

A cross-section SEM image of untreated extruded aluminum is shown in Figure 4.19. This image illustrates an aluminum piece cast in epoxy, with the epoxy bulk visible at the top and the aluminum bulk at the bottom. The intermediate layer exhibits signs of an oxide layer, as indicated by the presence of aluminum and oxygen according to EDX analysis, shown in Figure 4.20. However, upon examining the chemical composition in spectrum 2 and 4, several elements, including large amounts of silicon and carbon, were detected. The presence of these can be attributed to residues from the polishing stage, likely stemming from a crack in the epoxy where polishing residue could be trapped. Additionally, the detection of various other elements suggests potential cross-contamination from grinding and polishing consumables if not thoroughly cleaned by previous users. Additional spectrum 1, 3, 5 and 6 are found in Appendix A.3. In the figure, the oxide layer is not visible due to insufficient resolution at the required magnification of the SEM instrument utilized. Consequently, no further samples were examined.

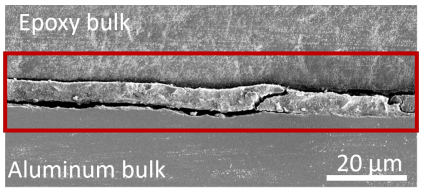

Figure 4.19: Cross-section SEM image of untreated extruded aluminum.

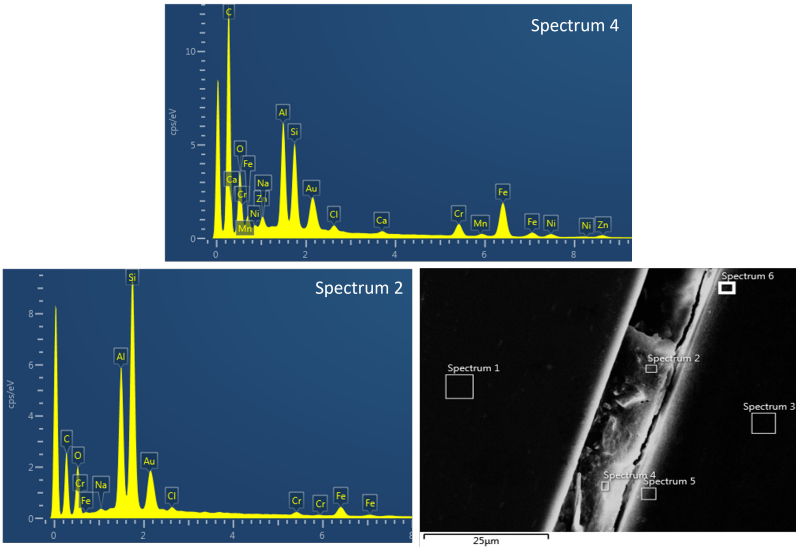

Figure 4.20: EDX analysis of untreated extruded aluminum.

4.6 X-ray Photoelectron Spectroscopy

XPS results are displayed in figures showing atomic percent at different sputter depths in reference to Ta_2O_5. Common for all initial survey scans, is that the aluminum is found in its metallic and oxidized form, where the oxidized form is as expected, dominating. Oxygen is found in metallic form and as metallic hydroxide, where the hydroxide is most likely due to moisture in air. Large amounts of contaminants were found on the untreated material, and smaller quantities were also found on the treated samples. For the aluminum sheet, the dominating contaminants were carbon, fluoride and phosphorus, whilst extruded material had carbon and chloride as contaminants. Carbon is highly abundant in the environment, and therefore hard to avoid using extremely surface sensitive instruments.

Surveys were also performed at the sputtered condition at 100 nm for all samples except untreated extruded aluminum where the sputtered condition was at 20 nm. Final surveys are showing argon implementation, simply because the ion beam used for sputtering is generated with an argon ion gun. Further, the dominating aluminum peak is in its metallic state, suggesting that the oxide has disintegrated into islandic form. No contaminants were found at the sputtered condition.

4.6.1 Aluminum sheet

4.6.1.1 Untreated

The result from XPS analysis of untreated aluminum sheet is shown in Figure 4.21. The oxide thickness can be estimated to 3 nm when converted to a scale for Al_2O_3.

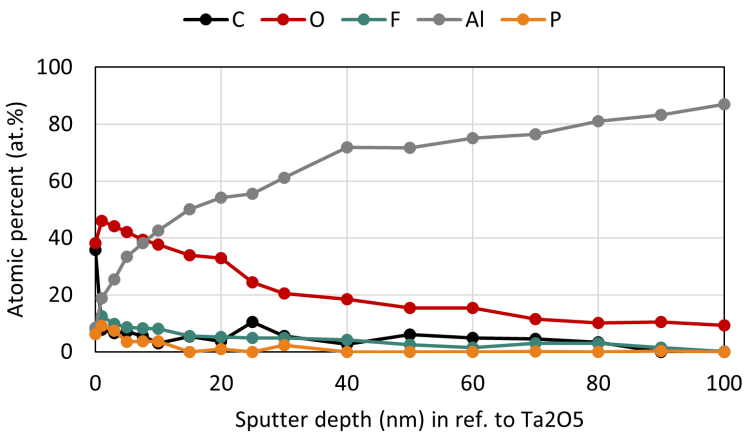

Figure 4.21: Depth profile of untreated aluminum sheet showing the atomic percent of C, O, F, Al and P.

Initial and final survey scans, as well as narrow scans are shown in Figure A.8 and A.9 in Appendix A.4.1. Results for the initial state are showing F and P are present as metallic fluorine and phosphorous. Small amounts of silicon, titanium, calcium, and magnesium is also found. The uppermost oxide could hence be a pentary type, *i.e.* Al-Si-Ti-Ca-Mg-O. An explanation for this could be that the coupons are two years old and the environments it has been exposed to are unknown. At the final state, a small amount of fluorine and iodide are unexpectedly detected in metallic form, and is most likely contaminants.

4.6.1.2 T2

The result from XPS analysis of aluminum sheet treated with T2 laser parameter is shown in Figure 4.21. The oxide thickness can be estimated to 55 nm when converted to a scale for Al_2O_3.

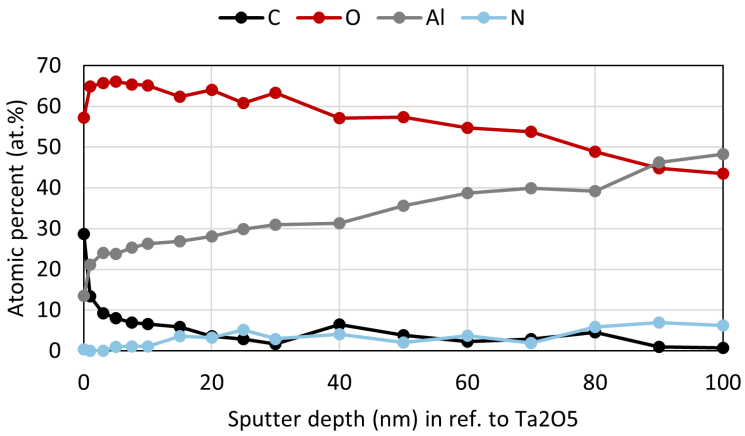

Figure 4.22: Depth profile of aluminum sheet treated with laser parameter T2 showing the atomic percent of C, O, Al and N.

Initial and final survey scans, as well as narrow scans are shown in Figure A.10 and A.11 in Appendix A.4.1. At the initial state, carbon was detected and supposed to be contamination. For the final condition, nitrogen is detected, indicated by a peak at 397 eV, suggesting the formation of a metal nitride, in this case aluminum nitride. This phenomenon may arise from nitridation on the alloy surface, facilitated by the high temperatures induced by laser spots [72], compounded by the abundance of nitrogen in the atmosphere (approximately 78%). A possible explanation could be the slow speed and a large %overlap, allowing nitrogen to diffuse into the melted material and incorporating into the Al forming aluminum nitride.

4.6.1.3 H2

The result from XPS analysis of aluminum sheet treated with H2 laser parameter is shown in Figure 4.21. The oxide thickness can be estimated to 25 nm when converted to a scale for Al_2O_3.

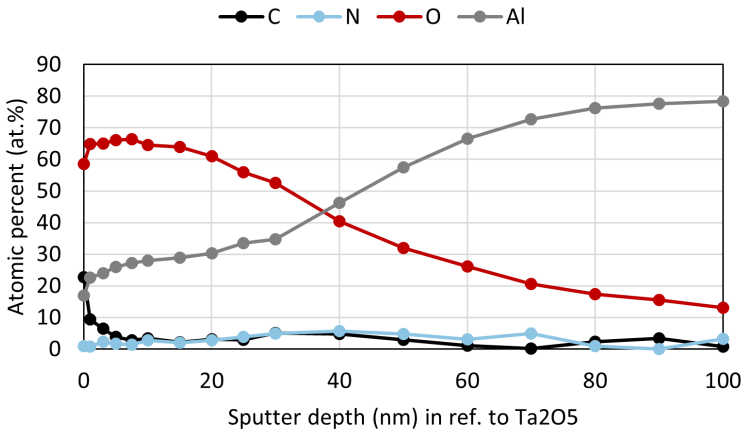

Figure 4.23: Depth profile of aluminum sheet treated with laser parameter H2 showing the atomic percent of C, N, O and Al.

Figure A.12 and A.11 in Appendix A.4.1 present the initial and final survey scans, as well as narrow scans for this sample. In the initial survey, carbon and fluoride (in metal fluoride form) are detected and supposed to be contaminants. Further, small quantities of magnesium were detected, however they fell below the detection limit and thus hinder proper characterization. At the sputtered condition, the carbon and fluoride are diminished.

4.6.2 Extruded aluminum

4.6.2.1 Untreated

The result from XPS analysis of untreated extruded aluminum is shown in Figure 4.24. The oxide thickness can be estimated to 4 nm when converted to a scale for Al_2O_3. This confirms that the intermediate layer in the SEM image in Figure 4.19 does not

display the oxide layer. The cause of the difference stems from the sample preparation as explained in Section 4.5.1.

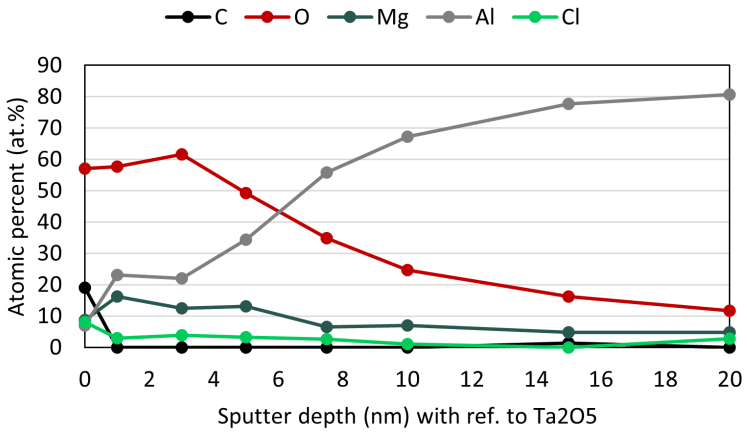

Figure 4.24: Depth profile of untreated extruded aluminum showing the atomic percent of C, O, Mg, Al and Cl.

Figure A.14 and A.15 in Appendix A.4.2 show initial and final survey scans as well as narrow scans. It can be seen for the initial state, that magnesium is present in an oxidized state, whereas aluminum is present in both an oxidized and in metallic state. This indicates that the oxide is bimetallic, consisting of aluminum and magnesium. The results after sputtering shows that the uniform oxide layer is almost removed, or disintegrated into islandic form.

4.6.2.2 T2

The result from sample extruded aluminum treated with parameter T2 is displayed in Figure 4.25. The oxide layer was estimated to approximately 45 nm when converted to Al_2O_3.

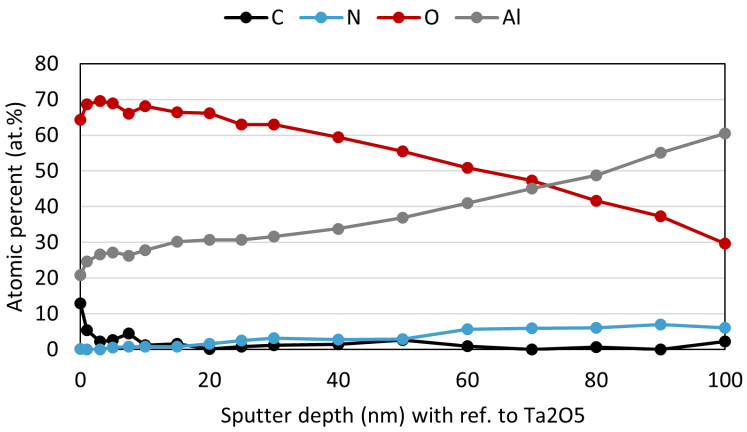

Figure 4.25: Depth profile of extruded aluminum treated with laser parameter T2 showing the atomic percent of C, N, O and Al.

At the onset, carbon, aluminum, and oxygen were detected, which can be seen in Figure A.16 in Appendix A.4.2. The carbon, as previously noted, is a contaminant. At the final condition, presented in Figure A.17, nitrogen is detected, most likely due to nitridation, as also seen for the aluminum sheet treated with T2.

4.6.2.3 H6

The result for extruded aluminum treated with H6 is shown in Figure 4.26. The figure displays the atomic percent of C, O, Mg, Al, and Cl at different sputter depths with reference to Ta_2O_5. Carbon and chlorine are present on the surface of the sample, which can be from contamination, as stated before. The oxide thickness can be estimated to 40 nm when converted to a scale for Al_2O_3.

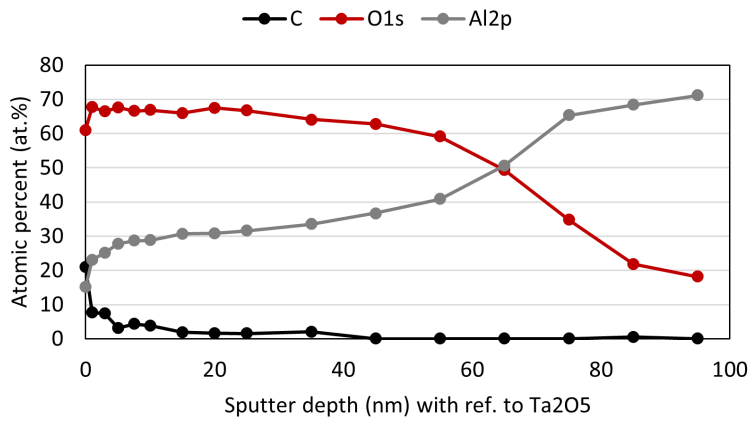

Figure 4.26: Depth profile of extruded aluminum treated with laser parameter H6 showing the atomic percent of C, O and Al.

From Figure A.18 in Appendix A.4.2, it can be seen that carbon and chlorine are present, which are likely to be contaminants as stated before. The results after sputtering are displayed in Figure A.19, shows that the uniform oxide layer is almost removed, or disintegrated into islandic form.

4.6.3 XPS and adhesion strength

Regarding the thickness of the alumina layer, T2 gives the thickest oxide of 55 nm and 45 nm for aluminum sheet and extruded respectively, followed by H2 and H6 with 25 nm and 40 nm, and lastly untreated resulted in 3 and 4 nm. A previous study has claimed that laser can thermally induce oxide growth [73]. Further, the oxide layer increases the -OH bonds, leading to improved wetting and enhanced adhesion [22]. This can be an explanation for why substrates treated with T2 shows higher lap shear strength than that of H2, H6, and the untreated material.

The removal of contaminants and grease can be another reason for improved adhesion [22]. This can be seen as the untreated aluminum sheet and extruded aluminum have 40 at% and 20 at% of carbon on the top layer of the surface, while

aluminum treated with T2 only has around 25 at% and 15 at%, showing that the laser treatment removes carbon based contaminants, and improves the bond strength. The high value of above 20 at% of carbon for H6 can be explained by the handling of the material when being cut into smaller pieces for XPS. This is supported by the low RFU and contact angle values for H6, followed by good lap shear results.

High concentrations of magnesium oxide in the oxide layer have previously been proposed to have a negative effect on adhesively bonded joints [74]. Since XPS measurements reveal that the oxide layer of untreated aluminum consists of magnesium oxide together with aluminum oxide, this could be a further explanation of why the untreated material shows weaker bond strength. Laser parameters T2 and H6 efficiently remove the magnesium oxide, increasing the bonding strength.

5
Conclusion

Upon completion of this project, it is clear that pre-treatment is necessary to achieve good adhesion and strengths for both unaged and aged samples. The laser is the predominant treatment method, as plasma was not sufficient for all adhesives. We can conclude that the T2 laser parameter was the best in general, as it provided good results for all specimen.

Regarding the surface properties, several conclusions were made. With laser treatment, cleaner surfaces were attained. The cleanliness of the surfaces was confirmed with RFU and contact angle measurements, showing a great positive impact on the adhesion. On the other hand, no apparent trend could be seen with surface roughness, and parameters such as Ssk might be of higher interest. Top view SEM-images revealed similar results to surface roughness, confirming that the structure is of greater importance than the roughness.

With cross-section SEM-images, it was not possible to visualize the oxide layer due to resolution limitations. However, XPS showed that laser treatment induces growth of the oxide layer. It can be concluded that a thicker oxide enhances adhesion, while high concentrations of magnesium in the oxide showed a negative impact on the adhesion. Furthermore, XPS confirmed the cleanliness results, where laser treated samples showed a decrease of contaminants, which resulted in improved adhesion. XPS also showed that laser parameter T2 induced nitridation, possibly due to the low speed of T2.

5.1 Further outlook

It is recommended to study new combinations of laser parameters, with a particular emphasis on achieving a high %overlap scan. Once an optimal combination of laser parameters is identified, visual inspection and RFU measurements could serve as quick and viable methods for quality control. These methods would enable efficient assessment of the surface treatment's effectiveness, ensuring consistent and reliable adhesive bonding in production. Other considerations and proposals for future work are presented in the following sections.

5.1.1 Further SEM analysis

Examining both the mechanical interlocking and the boundary layer formed by the adhesive in contact with the substrate could be a valuable next step to assess whether the adhesive adequately wets the surface. This can be done by looking after potential gaps where water could be trapped. Previous research by H. Wan et al. has demonstrated such investigations of the cross-sections of bonded substrates using SEM [75].

5.1.1.1 Transmission electron microscopy

Since SEM-analysis could not scan the surface to a high enough magnification for visually evaluating the aluminum oxide layer for all samples, a viable option could be using focused ion beam transmission electron microscopy (FIB-TEM) for this purpose. A previous study has successfully visualized a 10 nm aluminum oxide layer using FIB-TEM. However, the article also emphasized that XPS-analysis is a better option for determining chemical analysis of the oxide layer due to easier sample preparation and a cheaper analysis for industries [76].

5.1.2 Ageing testing

As previously noted, the ageing tests are conducted in an excessively severe environment, making them too harsh for precise evaluation of the adhesive properties in battery packs. To address this, there is a necessity to devise a new testing method that offers a more accurate assessment. A tropical environment with lower humidity could be one parameter worth evaluating, as such high humidities would lead to other problems such as electrical failure. It is important to recognize that the current testing technique is primarily designed for external vehicle parts, like car bodies, which are typically exposed to extreme weather conditions. Therefore, adapting the testing method to better suit the specific conditions encountered in tropical environments could lead to more relevant and reliable results.

Bibliography

[1] International Energy Agency, "World energy outlook 2023," 2023.

[2] United Nations, "The Paris Agreement."

[3] Volvo Cars, "Volvo Cars ska vara helt elektriskt senast 2030," 2021.

[4] R. Frenzel, T. Schiefer, I. Jansen, F. Simon, A. Calvimontes, K. Grundke, L. Häußler, and E. Beyer, "Polyelectrolytes to promote adhesive bonds of laser-structured aluminium," *International Journal of Adhesion and Adhesives*, vol. 61, pp. 35–45, Sept. 2015.

[5] B. Stojanovic, M. Bukvic, and I. Epler, "Application of Aluminum and Aluminum Alloys in Engineering," *Applied Engineering Letters : Journal of Engineering and Applied Sciences*, vol. 3, no. 2, pp. 52–62, 2018.

[6] F. Cavezza, M. Boehm, H. Terryn, and T. Hauffman, "A Review on Adhesively Bonded Aluminium Joints in the Automotive Industry," *Metals*, vol. 10, p. 730, June 2020.

[7] L. Romoli, F. Moroni, and M. Khan, "A study on the influence of surface laser texturing on the adhesive strength of bonded joints in aluminium alloys," *CIRP Annals*, vol. 66, no. 1, pp. 237–240, 2017.

[8] G. Rotella, M. Alfano, T. Schiefer, and I. Jansen, "Enhancement of static strength and long term durability of steel/epoxy joints through a fiber laser surface pretreatment," *International Journal of Adhesion and Adhesives*, vol. 63, pp. 87–95, Dec. 2015.

[9] G. Zhu, Z. Xu, Y. Jin, X. Chen, L. Yang, J. Xu, D. Shan, Y. Chen, and B. Guo, "Mechanism and application of laser cleaning: A review," *Optics and Lasers in Engineering*, vol. 157, p. 107130, Oct. 2022.

[10] Z. Xu, W. Yip, Z. Dong, M. Uddin, and G. Stevens, "On the laser surface pretreatment to enhance the surface texture, wettability and adhesion bonding strength of aluminium 7075-T6 laminates," *Composite Interfaces*, vol. 31, pp. 123–141, Jan. 2024.

[11] A. Rudawska and E. Jacniacka, "Analysis for determining surface free energy uncertainty by the Owen–Wendt method," *International Journal of Adhesion and Adhesives*, vol. 29, pp. 451–457, June 2009.

[12] B. Kronberg, K. Holmberg, and B. Lindman, *Surface chemistry of surfactants and polymers*. Chichester, West Sussex: Wiley, 2014.

[13] J. Durkee, "Using simple science to assay surface cleanliness," *Metal Finishing*, vol. 106, pp. 49–51, Feb. 2008.

[14] B. Duncan, R. Mera, D. Leatherdale, M. Taylor, and R. Musgrove, "Techniques for characterising the wetting, coating and spreading of adhesives on surface.," Techreport DEPC-MPR-020, National Physical Laboratory, Teddingtod, 2005.

[15] L. F. M. Da Silva, A. Öchsner, and R. D. Adams, "Introduction to Adhesive Bonding Technology," in *Handbook of Adhesion Technology* (L. F. M. Da Silva, A. Öchsner, and R. D. Adams, eds.), pp. 1–7, Berlin, Heidelberg: Springer Berlin Heidelberg, 2011.

[16] "Surface Tension and Its Measurement," in *Adhesives Technology Handbook*, pp. 21–36, Elsevier, 2009.

[17] A. Rudawska, "Mechanical treatment," in *Surface Treatment in Bonding Technology*, pp. 87–128, Elsevier, 2019.

[18] U. Nwaogu, N. Tiedje, and H. Hansen, "A non-contact 3D method to characterize the surface roughness of castings," *Journal of Materials Processing Technology*, vol. 213, pp. 59–68, Jan. 2013.

[19] Y. Boutar, S. Naïmi, S. Mezlini, L. F. M. Da Silva, M. Hamdaoui, and M. Ben Sik Ali, "Effect of adhesive thickness and surface roughness on the shear strength of aluminium one-component polyurethane adhesive single-lap joints for automotive applications," *Journal of Adhesion Science and Technology*, vol. 30, pp. 1913–1929, Sept. 2016.

[20] K. Uehara and M. Sakurai, "Bonding strength of adhesives and surface roughness of joined parts," *Journal of Materials Processing Technology*, vol. 127, pp. 178–181, Sept. 2002.

[21] I. A. Ashcroft and J. Comyn, "Effect of Water and Mechanical Stress on Durability," in *Handbook of Adhesion Technology* (L. F. M. Da Silva, A. Öchsner, and R. D. Adams, eds.), pp. 787–822, Berlin, Heidelberg: Springer Berlin Heidelberg, 2011.

[22] Y. Wu, J. Lin, B. E. Carlson, P. Lu, M. P. Balogh, N. P. Irish, and Y. Mei, "Effect of laser ablation surface treatment on performance of adhesive-bonded aluminum alloys," *Surface and Coatings Technology*, vol. 304, pp. 340–347, Oct. 2016.

[23] N. Saleema, D. Sarkar, R. Paynter, D. Gallant, and M. Eskandarian, "A simple surface treatment and characterization of AA 6061 aluminum alloy surface for adhesive bonding applications," *Applied Surface Science*, vol. 261, pp. 742–748, Nov. 2012.

[24] L. Wagner, "Mechanical surface treatments on titanium, aluminum and magnesium alloys," *Materials Science and Engineering: A*, vol. 263, pp. 210–216, May 1999.

[25] V. Gold, ed., *The IUPAC Compendium of Chemical Terminology: The Gold Book*. Research Triangle Park, NC: International Union of Pure and Applied Chemistry (IUPAC), 4 ed., 2019.

[26] S. Scott, Z. Islam, J. Allen, T. Yingnakorn, A. Alflakian, J. Hathaway, A. Rastegarpanah, G. D. Harper, E. Kendrick, P. A. Anderson, J. Edge, L. Lander, and A. P. Abbott, "Designing lithium-ion batteries for recycle: The role of adhesives," *Next Energy*, vol. 1, p. 100023, June 2023.

[27] P. E. Adhesives, "One component or two?," 2010.

[28] K.-B. Sim, T.-H. Lee, G.-Y. Han, and H.-J. Kim, "Thermal expansion and mechanical properties of urethane-modified epoxy bonded CFRP/steel joints at low and high temperatures for automotive," *Composite Structures*, vol. 322, p. 117426, Oct. 2023.

[29] D. A. Dillard, "Improving adhesive joint design using fracture mechanics," in *Advances in Structural Adhesive Bonding*, pp. 350–388, Elsevier, 2010.

[30] A. Pizzi and K. L. Mittal, *Handbook of adhesive technology*. New York (N. Y.): Marcel Dekker, 2nd ed., rev. and expanded ed., 2003.
[31] F. C. Campbell, *Structural composite materials*. Materials Park, Ohio: ASM Internat, 1. print ed., 2010.
[32] C. A. Harper, ed., *Modern plastics handbook*. New York: McGraw-Hill, 2000.
[33] R. G. Schmidt and J. P. Bell, "Epoxy adhesion to metals," in *Epoxy Resins and Composites II* (K. Dušek, ed.), vol. 75, pp. 33–71, Berlin/Heidelberg: Springer-Verlag, 1986. Series Title: Advances in Polymer Science.
[34] B. De Neve and M. E. R. Shanahan, "Physical and Chemical Effects in An Epoxy Resin Exposed to Water Vapour," *The Journal of Adhesion*, vol. 49, pp. 165–176, Apr. 1995.
[35] M. Dunky and A. Pizzl, "Wood adhesives," in *Adhesion Science and Engineering*, pp. 1039–1103, Elsevier, 2002.
[36] J. Comyn, "What are adhesives and sealants and how do they work?," in *Adhesive Bonding*, pp. 41–78, Elsevier, 2021.
[37] B. Duncan, "Developments in testing adhesive joints," in *Advances in Structural Adhesive Bonding*, pp. 389–436, Elsevier, 2010.
[38] S. Liu, X. Cheng, Q. Zhang, J. Zhang, J. Bao, and X. Guo, "An investigation of hygrothermal effects on adhesive materials and double lap shear joints of CFRP composite laminates," *Composites Part B: Engineering*, vol. 91, pp. 431–440, Apr. 2016.
[39] N. Mumtaz, Y. Li, R. Artiaga, Z. Farooq, A. Mumtaz, Q. Guo, and F.-U. Nisa, "Fillers and methods to improve the effective (out-plane) thermal conductivity of polymeric thermal interface materials – A review," *Heliyon*, vol. 10, p. e25381, Feb. 2024.
[40] M. Tisza and Z. Lukács, "High strength aluminum alloys in car manufacturing," *IOP Conference Series: Materials Science and Engineering*, vol. 418, p. 012033, Sept. 2018.
[41] M. Baruah and A. Borah, "Processing and precipitation strengthening of 6xxx series aluminium alloys: A review," *International Journal of Materials Science*, vol. 1, pp. 40–48, Jan. 2020.
[42] W. Liang, P. Rometsch, L. Cao, and N. Birbilis, "General aspects related to the corrosion of 6xxx series aluminium alloys: Exploring the influence of Mg/Si ratio and Cu," *Corrosion Science*, vol. 76, pp. 119–128, Nov. 2013.
[43] G. Straffelini, "Rolling," in *Ductility and Formability of Metals*, pp. 325–348, Elsevier, 2023.
[44] G. Straffelini, "Extrusion," in *Ductility and Formability of Metals*, pp. 349–364, Elsevier, 2023.
[45] E. McCafferty, *Introduction to Corrosion Science*. New York, NY: Springer New York, 2010.
[46] W. Wang, J. W. Xu, X. Chen, Y. J. Liang, and L. Z. Zhu, "The effect of laser surface treatment on the adhesive bonding performance of aluminum alloy," *Journal of Physics: Conference Series*, vol. 1605, p. 012136, Aug. 2020.
[47] J. M. Hollas, *Modern spectroscopy*. Chichester ; Hoboken, NJ: J. Wiley, 4th ed ed., 2004.

[48] M. Langer, R. Rechner, M. Thieme, I. Jansen, and E. Beyer, "Surface analytical characterisation of Nd:YAG-laser pre-treated Al Mg3 as a preparation for bonding," *Solid State Sciences*, vol. 14, pp. 926–935, July 2012.
[49] M. Naeem, "Laser Processing of Reflective Materials: A new technology managing reflection effects," *Laser Technik Journal*, vol. 10, pp. 18–20, Jan. 2013.
[50] RISE Research Institutes of Sweden, "Plasma surface modifications."
[51] Plasmatreat, "What is plasma," 2024.
[52] P. Chu, "Plasma-surface modification of biomaterials," *Materials Science and Engineering: R: Reports*, vol. 36, pp. 143–206, Mar. 2002.
[53] C. Tendero, C. Tixier, P. Tristant, J. Desmaison, and P. Leprince, "Atmospheric pressure plasmas: A review," *Spectrochimica Acta Part B: Atomic Spectroscopy*, vol. 61, pp. 2–30, Jan. 2006.
[54] Dyne Testing Ltd, "Metal Cleanliness Testing," 2024.
[55] D. L. Williams and T. M. O'Bryon, "Cleanliness Verification on Large Surfaces," in *Developments in Surface Contamination and Cleaning*, pp. 163–181, Elsevier, 2013.
[56] G. Mabilleau and A. Sabokbar, "In vitro biological test methods to evaluate bioresorbability," in *Degradation Rate of Bioresorbable Materials*, pp. 145–160, Elsevier, 2008.
[57] M. K. Singh and A. Singh, "Scanning electron microscope," in *Characterization of Polymers and Fibres*, pp. 387–419, Elsevier, 2022.
[58] L. Smart and E. Moore, *Solid state chemistry: an introduction.* Boca Raton: CRC Press, 4th ed ed., 2012.
[59] M. Nasrollahzadeh, M. Atarod, M. Sajjadi, S. M. Sajadi, and Z. Issaabadi, "Plant-Mediated Green Synthesis of Nanostructures: Mechanisms, Characterization, and Applications," in *Interface Science and Technology*, vol. 28, pp. 199–322, Elsevier, 2019.
[60] R. H. Geiss, "EDS," in *Encyclopedia of Materials Characterization*, pp. 120–134, Elsevier, 1992.
[61] L. Levit and A. Steinman, "ESD Controls in Cleanroom Environments," in *Developments in Surface Contamination and Cleaning*, pp. 173–195, Elsevier, 2008.
[62] H. Seyama, M. Soma, and B. Theng, "X-Ray Photoelectron Spectroscopy," in *Developments in Clay Science*, vol. 5, pp. 161–176, Elsevier, 2013.
[63] M. Omidi, A. Fatehinya, M. Farahani, Z. Akbari, S. Shahmoradi, F. Yazdian, M. Tahriri, K. Moharamzadeh, L. Tayebi, and D. Vashaee, "Characterization of biomaterials," in *Biomaterials for Oral and Dental Tissue Engineering*, pp. 97–115, Elsevier, 2017.
[64] J. Lancaster, "The use of adhesives for making structural joints," in *Metallurgy of Welding*, pp. 54–84, Elsevier, 1999.
[65] D. Dos Santos, D. Carastan, L. Tavares, and G. Batalha, "Polymeric Materials Characterization and Modeling," in *Comprehensive Materials Processing*, pp. 37–63, Elsevier, 2014.
[66] S. Ebnesajjad, "Theories of Adhesion," in *Surface Treatment of Materials for Adhesive Bonding*, pp. 77–91, Elsevier, 2014.

[67] R. Cruz, L. Correia, S. Cabral-Fonseca, and J. Sena-Cruz, "Durability of bond of EBR CFRP laminates to concrete under real-time field exposure and laboratory accelerated ageing," *Construction and Building Materials*, vol. 377, p. 131047, May 2023.

[68] L. Bónová, W. Zhu, D. K. Patel, D. V. Krogstad, and D. N. Ruzic, "Atmospheric pressure microwave plasma for aluminum surface cleaning," *Journal of Vacuum Science & Technology A: Vacuum, Surfaces, and Films*, vol. 38, p. 023002, Mar. 2020.

[69] H. Li, A. Belkind, F. Jansen, and Z. Orban, "An in situ XPS study of oxygen plasma cleaning of aluminum surfaces," *Surface and Coatings Technology*, vol. 92, pp. 171–177, July 1997.

[70] G. Schnell, U. Duenow, and H. Seitz, "Effect of Laser Pulse Overlap and Scanning Line Overlap on Femtosecond Laser-Structured Ti6Al4V Surfaces," *Materials*, vol. 13, p. 969, Feb. 2020.

[71] Keyance, "Ssk (Skewness) | Area Roughness Parameters."

[72] P. Schaaf, "Laser nitriding of metals," *Progress in Materials Science*, vol. 47, pp. 1–161, Jan. 2002.

[73] R. Rechner, I. Jansen, and E. Beyer, "Influence on the strength and aging resistance of aluminium joints by laser pre-treatment and surface modification," *International Journal of Adhesion and Adhesives*, vol. 30, pp. 595–601, Oct. 2010.

[74] O. Lunder, B. Olsen, and K. Nisancioglu, "Pre-treatment of AA6060 aluminium alloy for adhesive bonding," *International Journal of Adhesion and Adhesives*, vol. 22, pp. 143–150, Jan. 2002.

[75] H. Wan, J. Min, and J. Lin, "Experimental and theoretical studies on laser treatment strategies for improving shear bonding strength of structural adhesive joints with cast aluminum," *Composite Structures*, vol. 279, p. 114831, Jan. 2022.

[76] R. Gruber, T. D. Singewald, T. M. Bruckner, L. Hader-Kregl, M. Hafner, H. Groiss, J. Duchoslav, and D. Stifter, "Investigation of Oxide Thickness on Technical Aluminium Alloys—A Comparison of Characterization Methods," *Metals*, vol. 13, p. 1322, July 2023.

A

Appendix 1

A.1 Cross-section sample preparation for SEM

Epoxy was prepared in a cup by mixing 25 parts EpoFix resin with 3 parts EpoFix hardener by weight. The coupons was covered with epoxy, and was left to cure in a fume hood over night. After the epoxy cured and was protecting the surfaces of the coupons, the coupons were cut into appropriate sized pieces (~2.5 cm) using a band and fine saw. The pieces were then immobilized standing upright in a plastic cup, which was filled with epoxy, prepared in the same way as previously.

The finished instillation was then polished using an automatic polisher, Struers Laboforce-100. The polishing was performed using sandpapers, starting with the roughest, and going down in roughness for each step. Water and chemical suspensions were automatically dispensed to minimize heating while polishing the samples. Polished samples, were investigated with an optical microscope to ensure sufficient polishing. Further, Leica EM ACE600 sputter coater was used to sputter about 11 nm layer of gold on the surface to make it conducting.

A.2 LSS curves

The LSS curves for AD1 and AD2 on aluminum sheet as well as AD3 and AD4 on extruded aluminum for unaged and aged samples and all the respective pre-treatments are shown in Figure A.1–A.4.

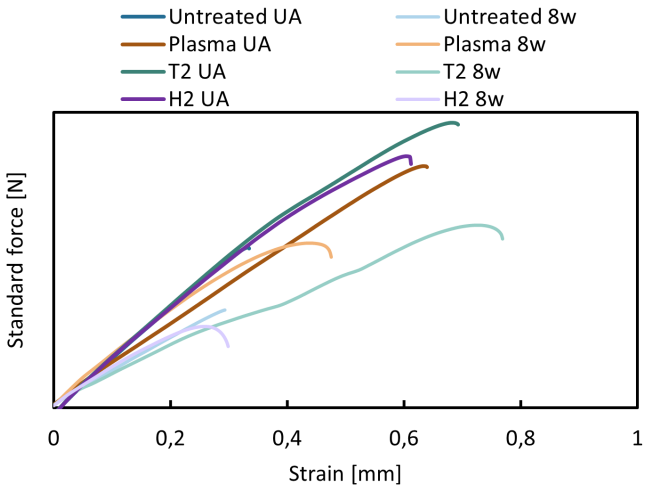

Figure A.1: Lap shear stress and strain curves for all the samples aged and not aged using the AD1 adhesive on aluminum sheet.

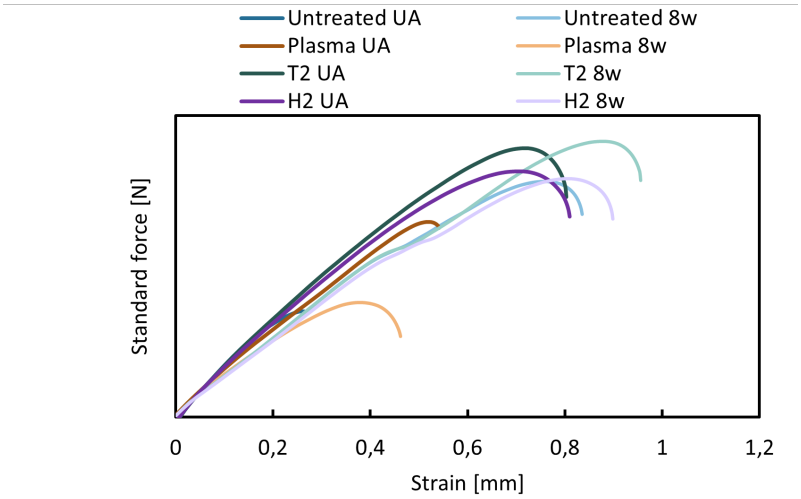

Figure A.2: LSS curves for unaged (UA) and eight weeks (8w) aged samples using the AD2 adhesive on aluminum sheet.

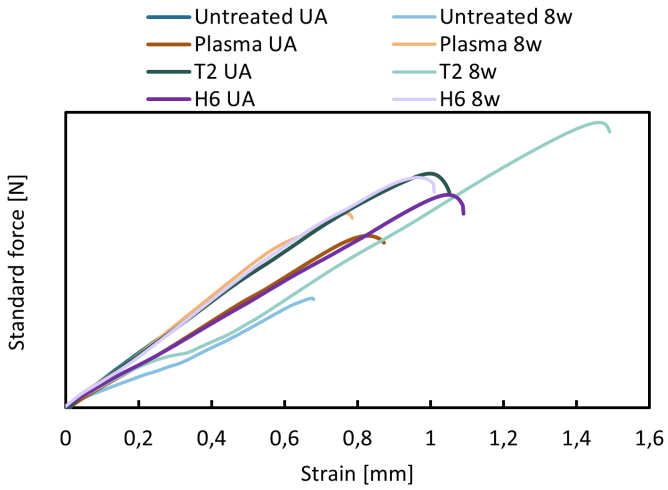

Figure A.3: LSS curves for unaged (UA) and eight weeks (8w) aged samples using the AD3 adhesive on extruded aluminum.

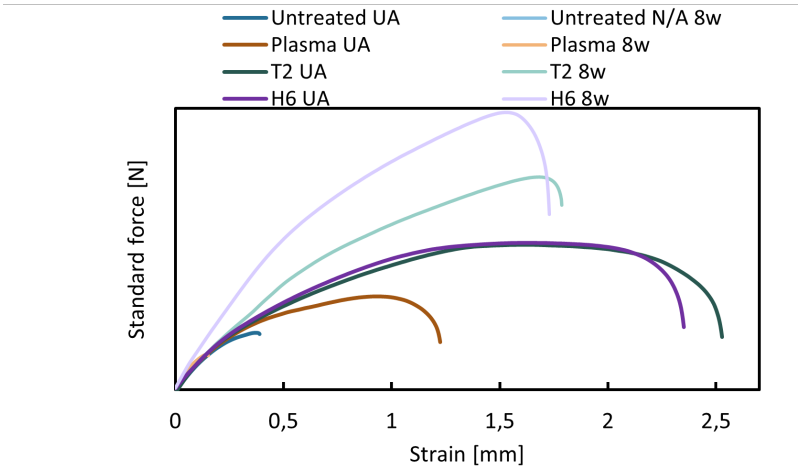

Figure A.4: LSS curves for unaged (UA) and eight weeks (8w) aged samples using the AD4 adhesive on extruded aluminum.

A.2.1 Failure modes

Failure modes of unaged aluminum sheet as well as extruded aluminum and their respective adhesives are shown in Figure A.5.

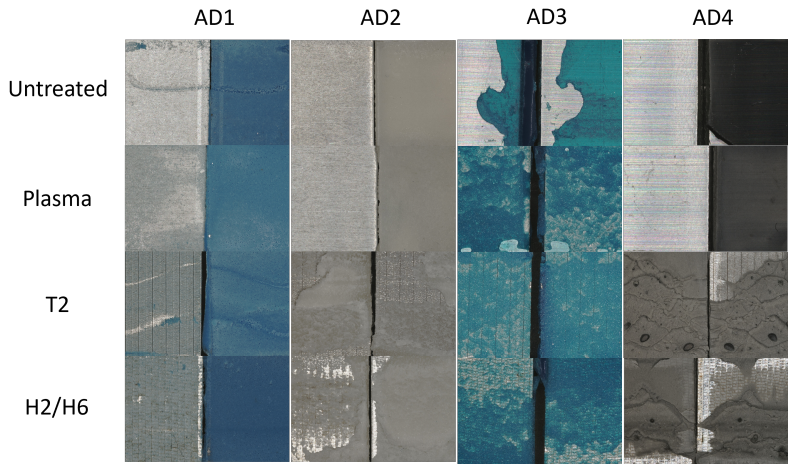

Figure A.5: Failure patterns after lap shear testing of unaged samples.

A.2.2 Ageing effects

The four-week ageing testing was exclusively conducted on the laser-treated sample as an additional method, considering that an eight-week test might be overly harsh. It is important to recognize that the humidity and temperature conditions within a battery environment could trigger more severe failures in the system than those observed in the adhesives. Therefore, there is a need to develop a new testing approach. It is also crucial to note that only a single measurement was taken during the four-week test, thus lacking statistically. The failure modes for four weeks testing are shown in Figure A.6

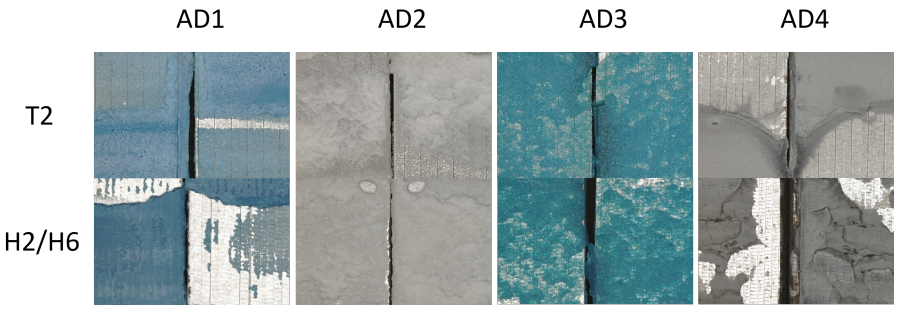

Figure A.6: Failure patterns after lap shear testing of samples being aged for four weeks.

A.3 SEM-EDX results

Additional EDX-spectras from Figure 4.20 can be found in Figure A.7. These spectras display the composition in the bulk material (aluminum) and the mounting material (epoxy).

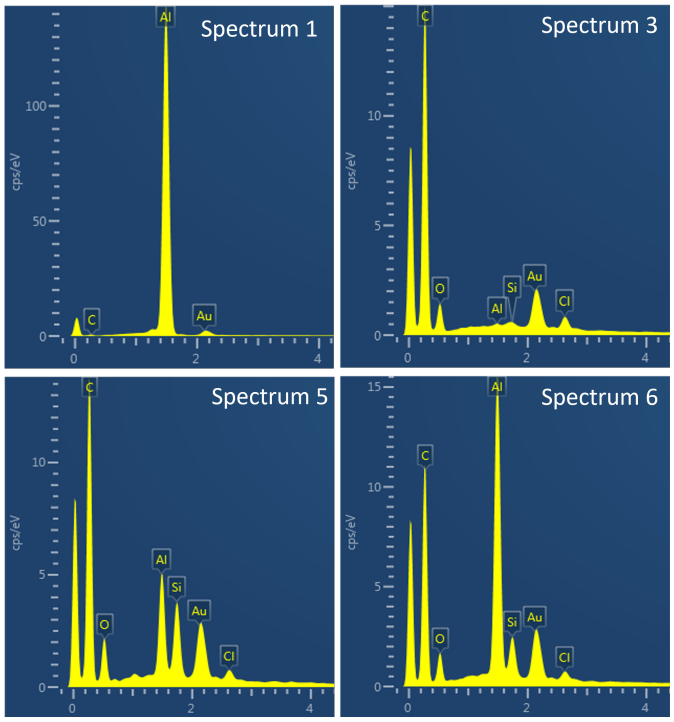

Figure A.7: EDX spectrum 4, 5, and 6 from Figure 4.20

A.4 XPS results

In this section, XPS-results from the survey and narrow scans for both the starting and the final condition are presented. The survey scans display the composition of elements found in the sample, and the narrow scans show the oxidized state of aluminum and oxygen.

A.4.1 Aluminum sheet

Initial survey scans are shown in Figure A.8–A.12. Results from the final survey and narrow scans after 100 nm sputtering are shown in Figure A.9–A.13.

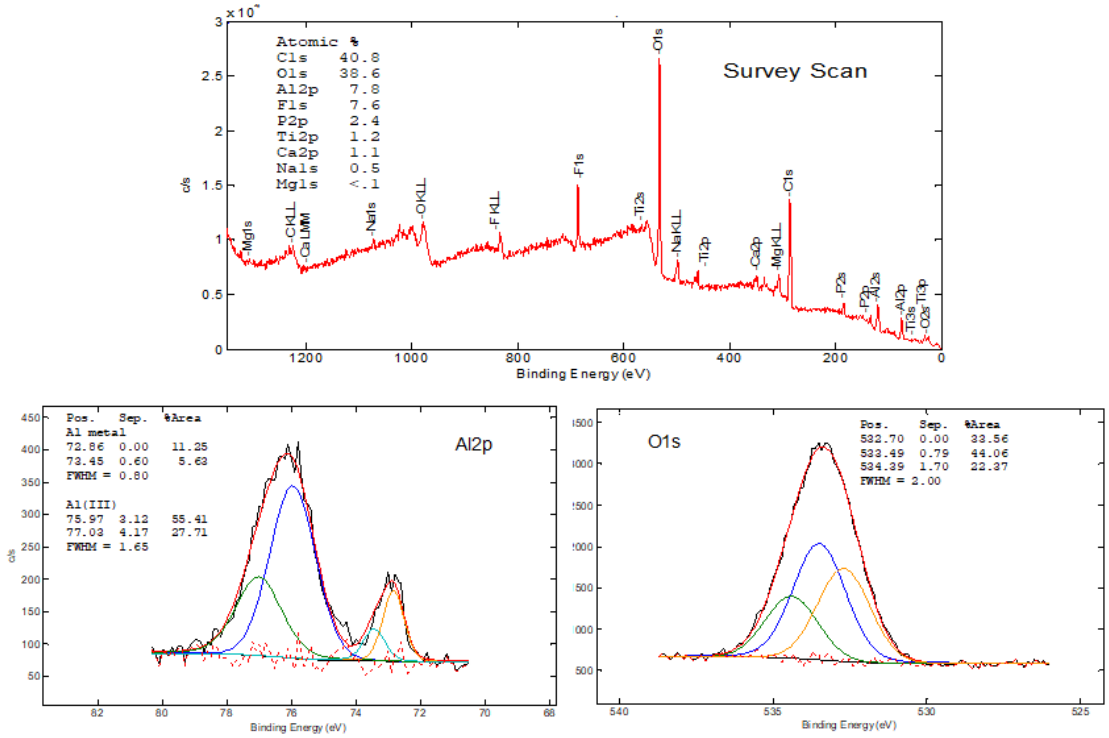

Figure A.8: Initial survey scan of the untreated aluminum sheet and narrow scans of respective individual element.

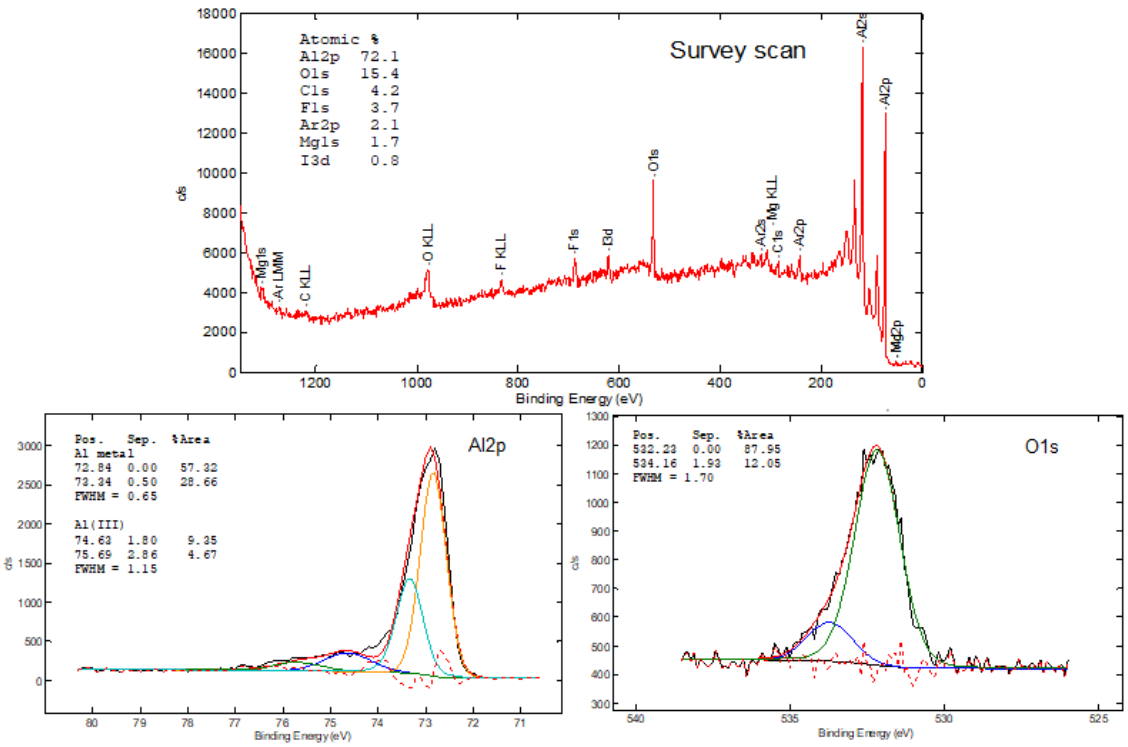

Figure A.9: Survey scan of the untreated aluminum sheet at the 100 nm sputtered conditions with narrow scans of respective individual element.

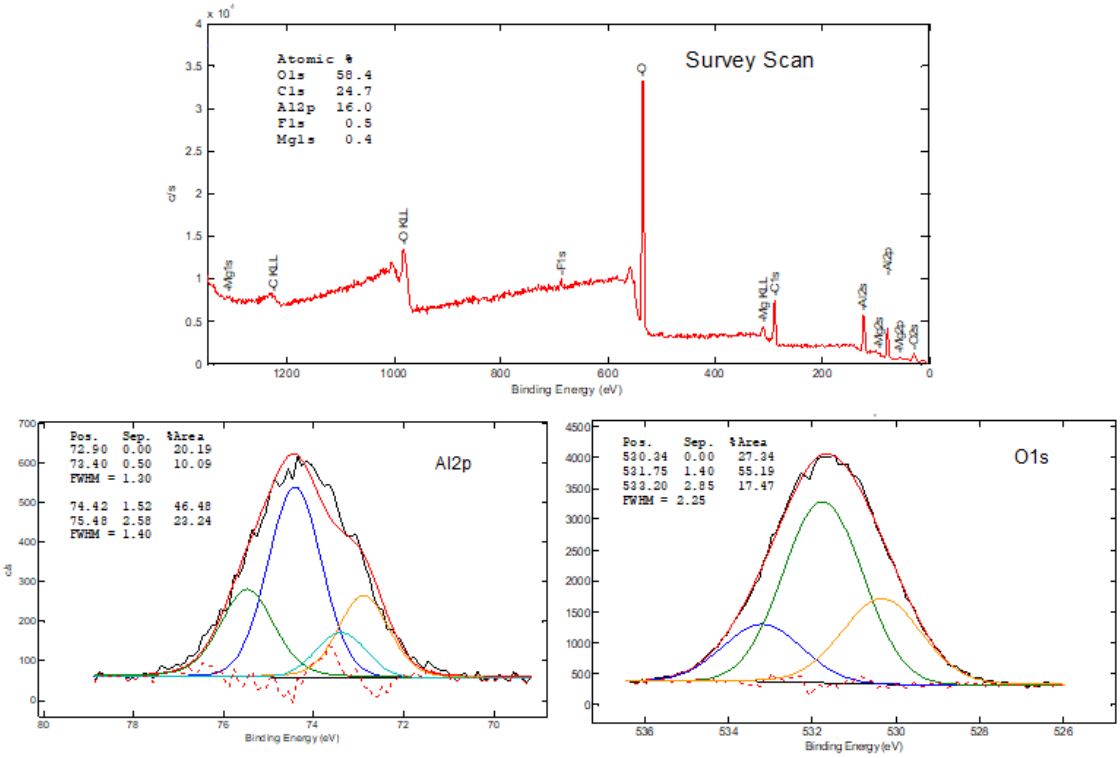

Figure A.10: Initial survey scan of T2 treated aluminum sheet and narrow scans of respective individual element.

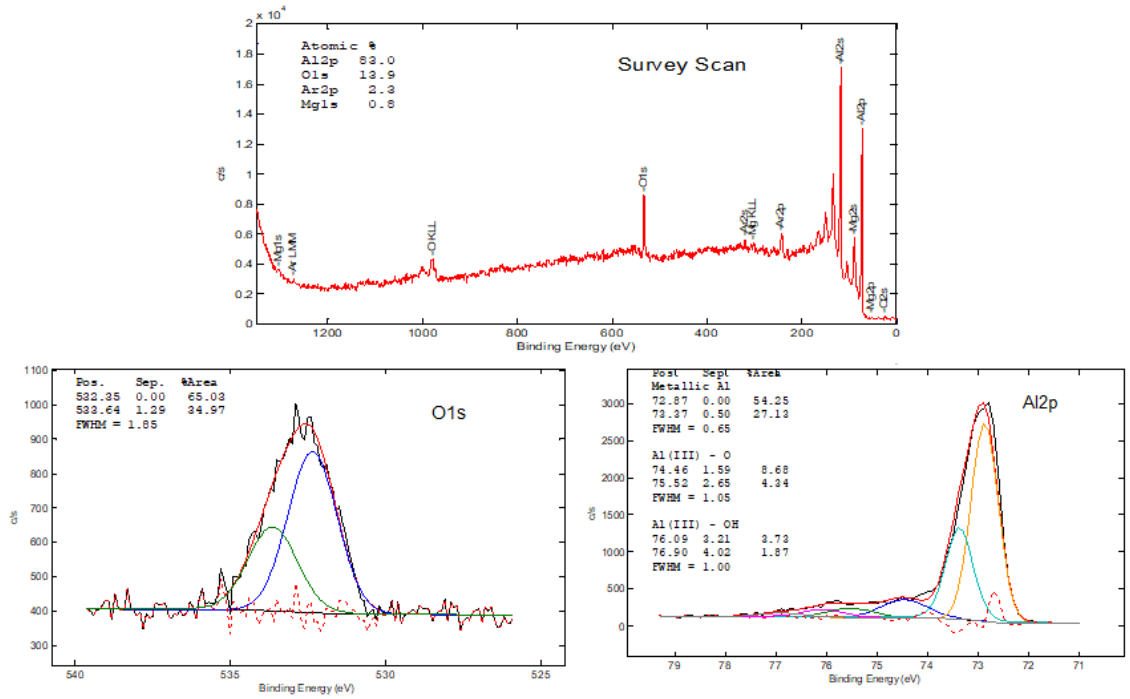

Figure A.11: Survey scan of T2 treated aluminum sheet at the 100 nm sputtered conditions with narrow scans of respective individual element.

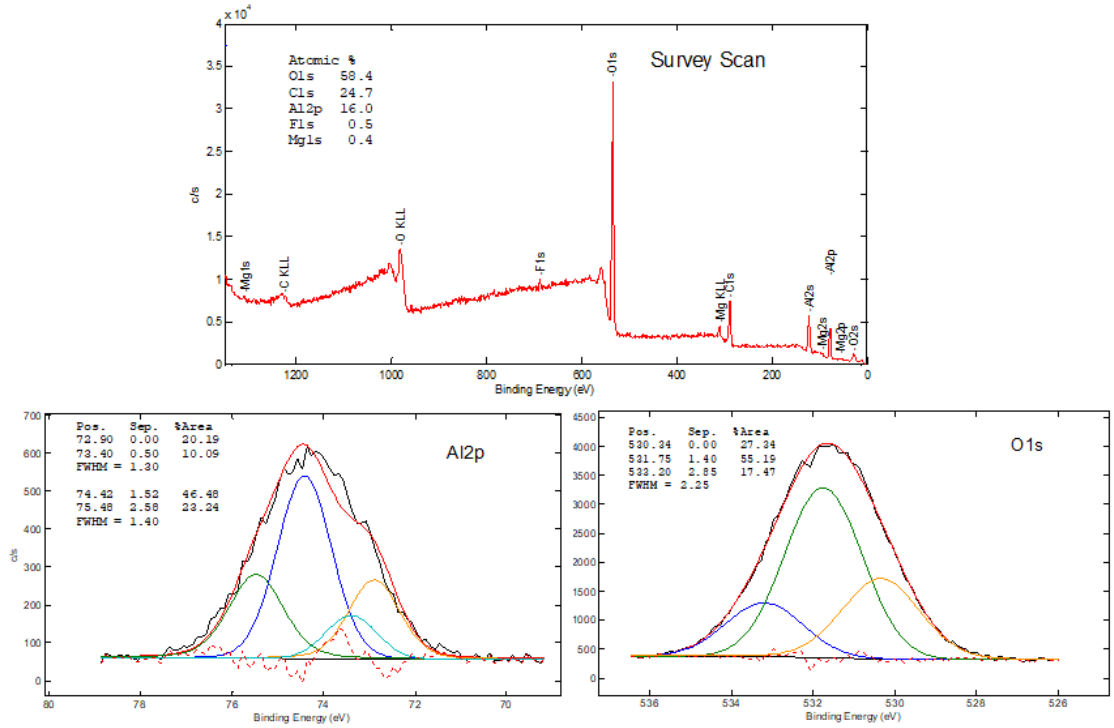

Figure A.12: Initial survey scan of H2 treated aluminum sheet and narrow scans of respective individual element.

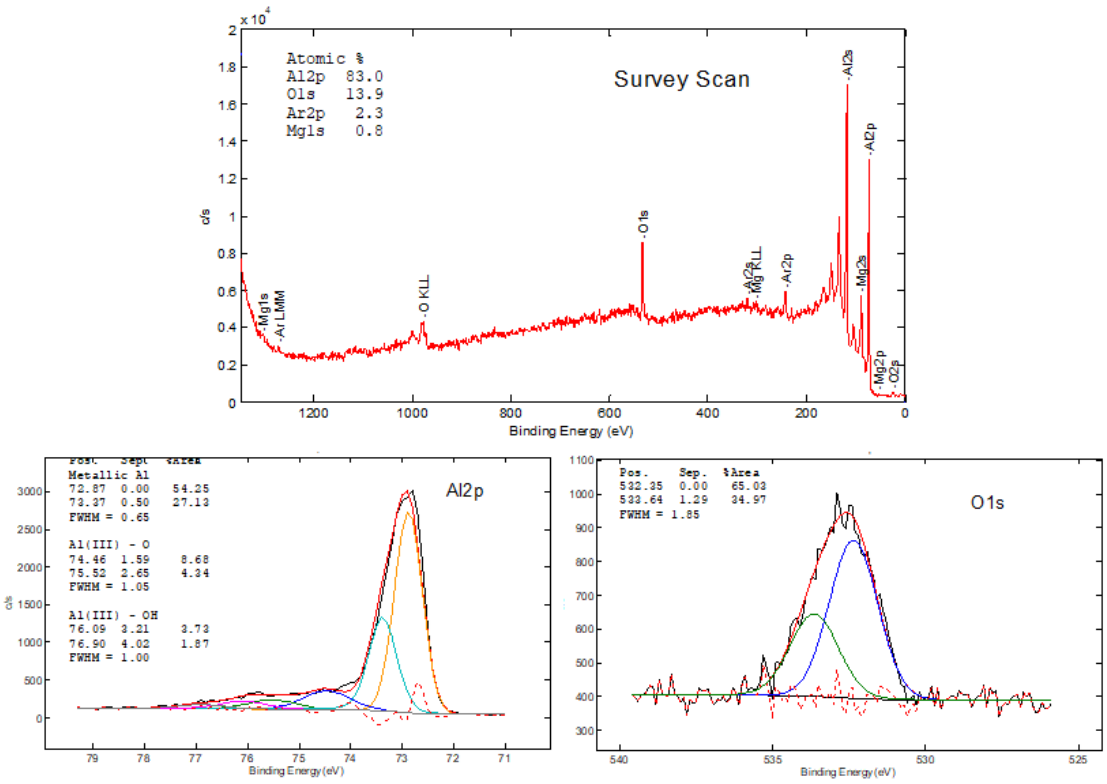

Figure A.13: Survey scan of H2 treated aluminum sheet at the 100 nm sputtered conditions with narrow scans of respective individual element.

A.4.2 Extruded aluminum

Initial survey scans are shown in Figure A.14–A.18. Results from the final survey and narrow scans after 100 nm sputtering are shown in Figure A.15–A.19.

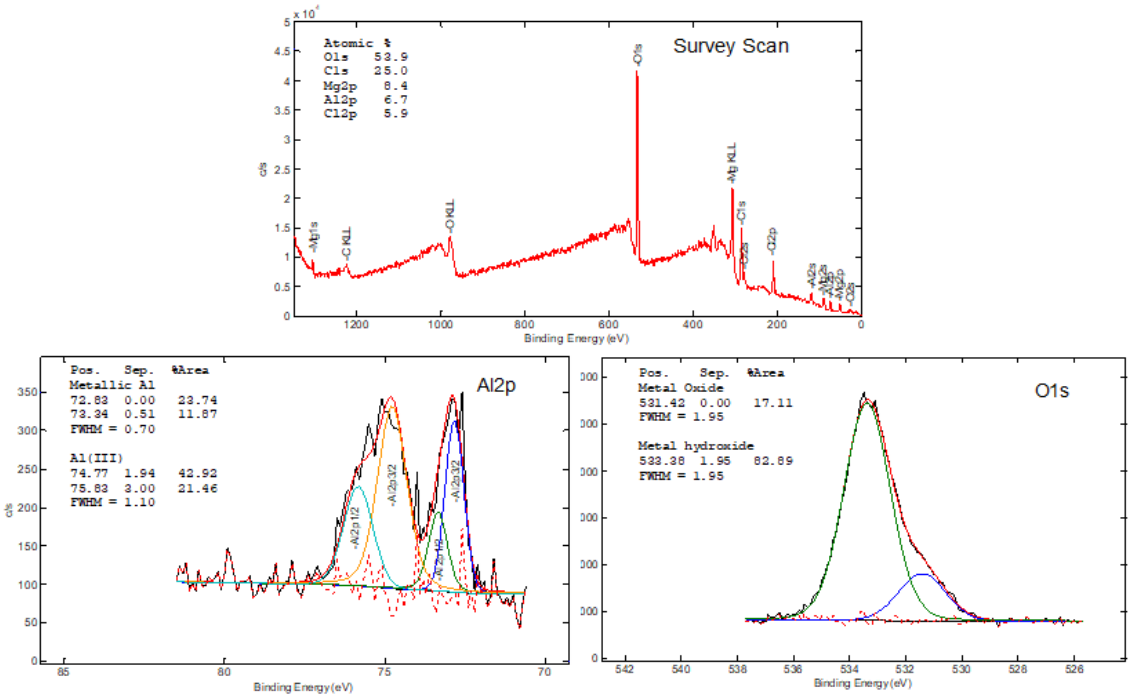

Figure A.14: Initial survey scan of the untreated extruded aluminum and narrow scans of respective individual element.

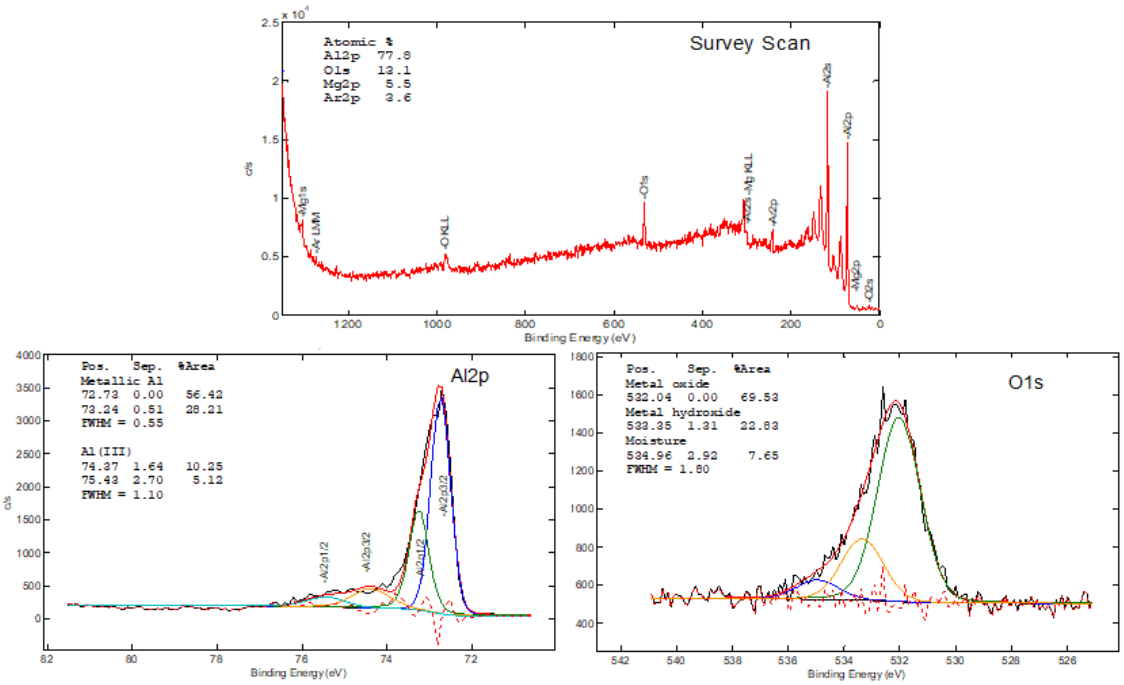

Figure A.15: Survey scan of the untreated extruded aluminum at the 20 nm sputtered conditions with narrow scans of respective individual element.

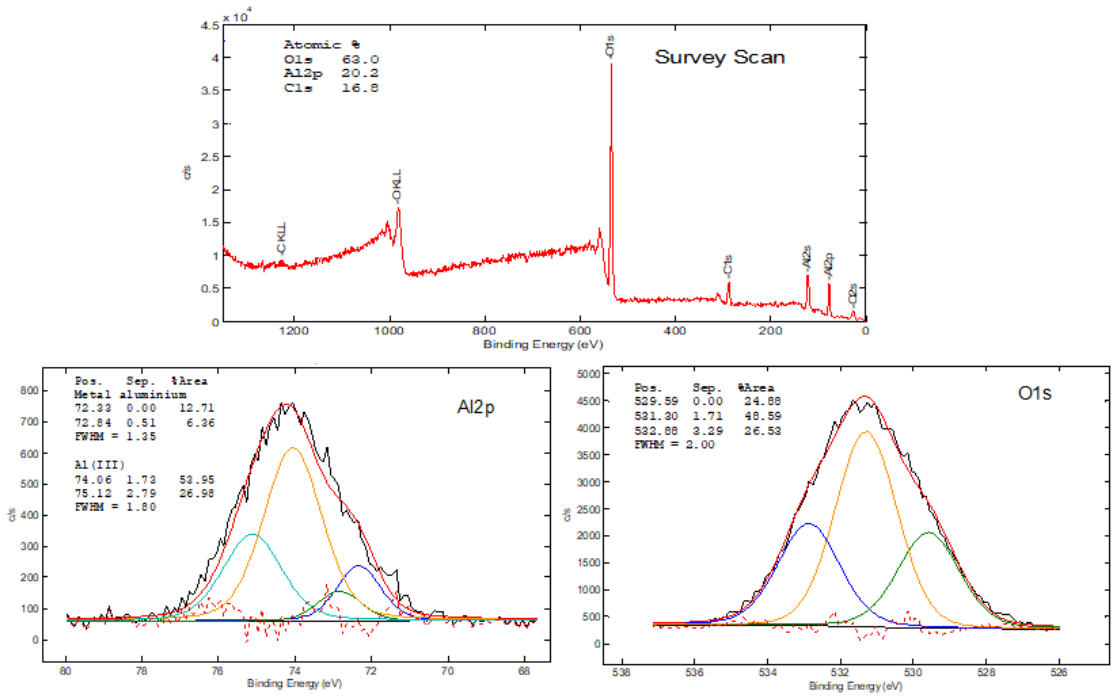

Figure A.16: Initial survey scan of the extruded aluminum treated with T2 and narrow scans of respective individual element.

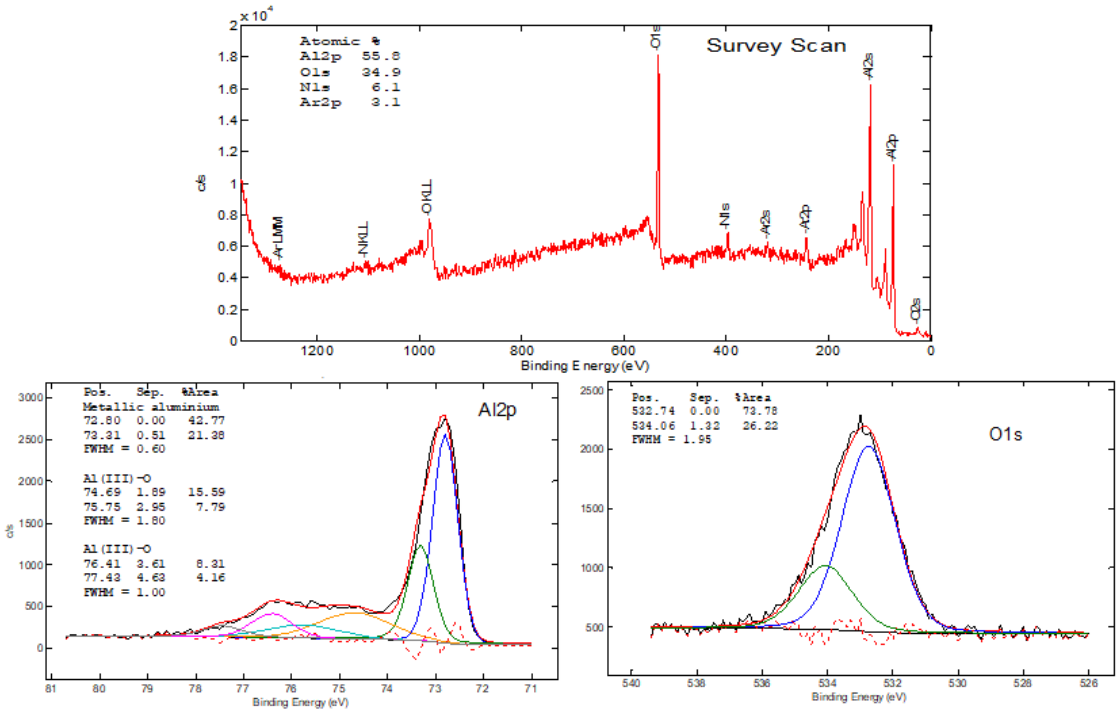

Figure A.17: Survey scan of the extruded aluminum treated with T2 at the 100 nm sputtered conditions with narrow scans of respective individual element.

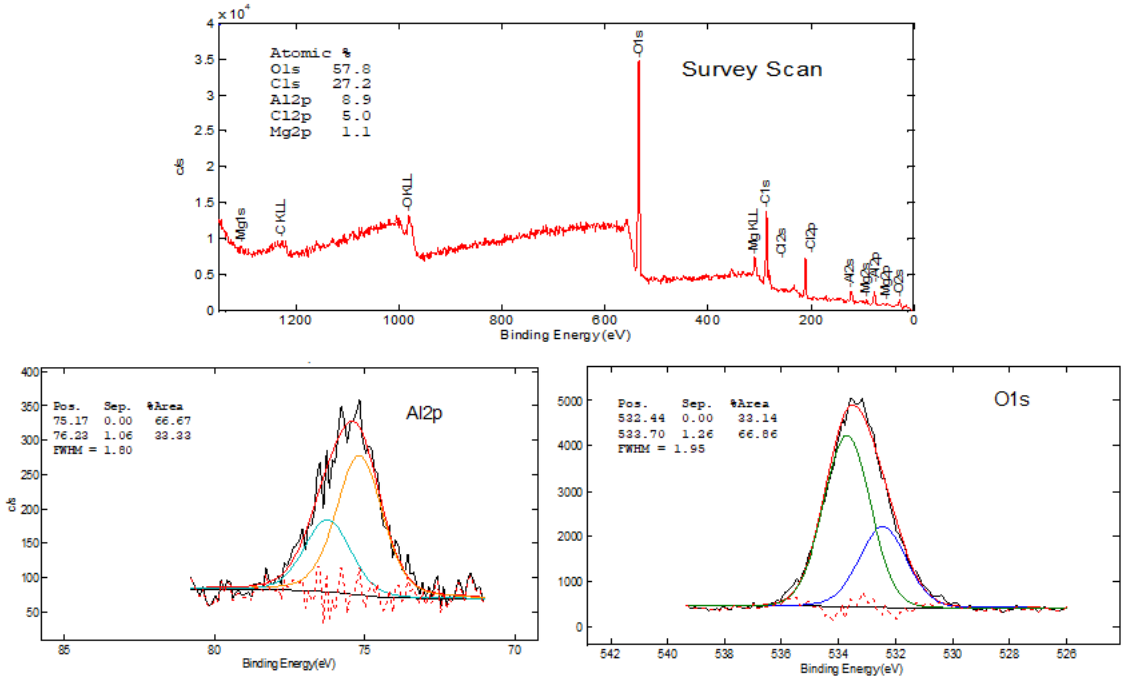

Figure A.18: Initial survey scan of the extruded aluminum treated with H6 and narrow scans of respective individual element.

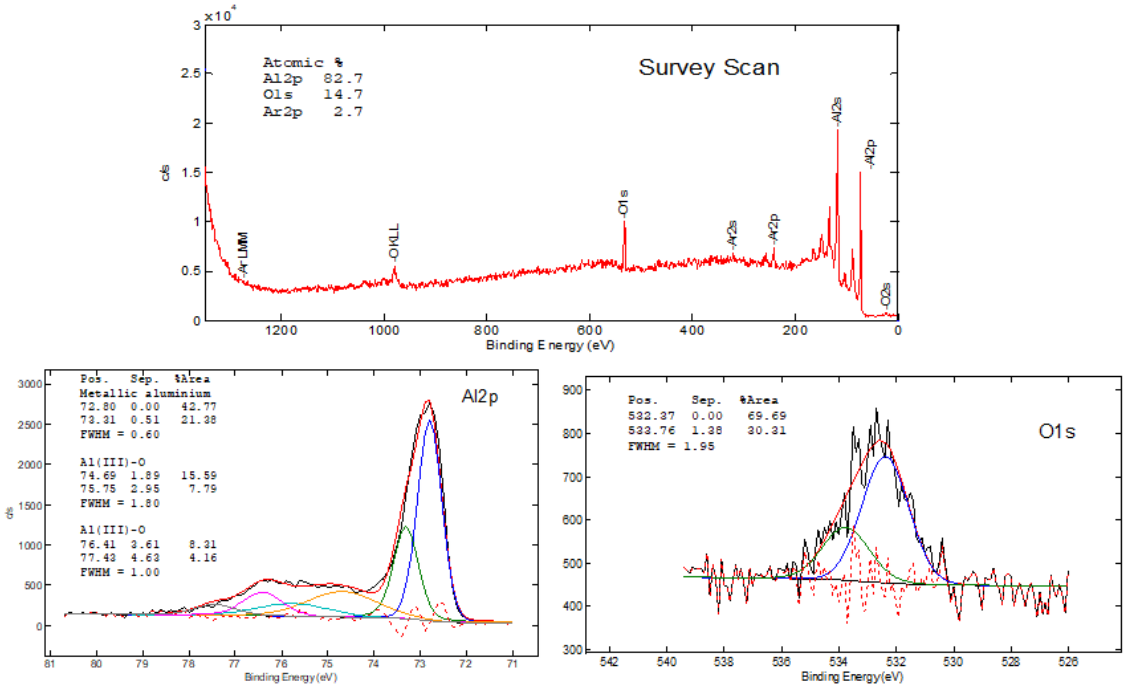

Figure A.19: Survey scan of the extruded aluminum treated with H6 at the 100 nm sputtered conditions with narrow scans of respective individual element.

B

Appendix 2

B.1 Environmental, societal, and ethical aspects

From an environmental perspective, laser pre-treatment can be considered a more sustainable alternative than chemical pre-treatment. It does not use any harmful chemicals that can pollute the air, water, or soil. Laser methods produce less waste and use less water, helping to conserve natural resources and reduce pollution.

This can be connected to societal aspects. Since people are becoming more and more concerned about the environment, businesses using cleaner technologies might gain a better reputation and attract more customers. This can overall help can support healthier communities in the long run.

From an ethical point of view, using lasers instead of chemicals can be safer for the employees. Chemicals can cause health problems like breathing issues and skin irritation. Lasers reduce these risks, making the workplace safer. This approach also aligns with ethical business practices by protecting workers' health and promoting sustainability.

DEPARTMENT OF SOME SUBJECT OR TECHNOLOGY
CHALMERS UNIVERSITY OF TECHNOLOGY
Gothenburg, Sweden
www.chalmers.se

CHALMERS
UNIVERSITY OF TECHNOLOGY